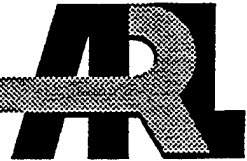


ARMY RESEARCH LABORATORY



Flight Mechanics of an Elastic Symmetric Missile

by Charles H. Murphy
and William H. Mermagen, Sr.

ARL-TR-2255

April 2000

20010604 084

Approved for public release; distribution is unlimited.

The findings in this report are not to be construed as an official Department of the Army position unless so designated by other authorized documents.

Citation of manufacturer's or trade names does not constitute an official endorsement or approval of the use thereof.

Destroy this report when it is no longer needed. Do not return it to the originator.

Army Research Laboratory

Aberdeen Proving Ground, MD 21005-5066

ARL-TR-2255

April 2000

Flight Mechanics of an Elastic Symmetric Missile

Charles H. Murphy

Weapons and Materials Research Directorate, ARL

William H. Mermagen, Sr.

Computational and Information Sciences Directorate, ARL

Abstract

The free-flight motion of an elastic missile is approximated with three bodies connected by two massless elastic cantilever beams. If the mass distribution of the three bodies is 1-2-1, the frequency of the symmetric oscillation of the outer bodies is within 5% of the classical frequency of the oscillation of a free-free beam. A second combined pitching antisymmetric flexing motion can occur with a frequency that is almost twice that of the symmetric flexing motion. As the beam stiffness is reduced, the symmetric flexing motion frequency approaches the rigid body aerodynamic zero-spin frequency, and the flight zero-spin aerodynamic frequency is considerably reduced. Moderate beam damping can cause dynamic instability for spins greater than the zero-spin aerodynamic frequency. Resonance mode amplification can occur when the spin is equal to the zero-spin aerodynamic frequency, but more importantly it can occur when the spin is equal to the two elastic flexing frequencies. Spin-yaw lock-in occurs at the lower elastic frequency.

Table of Contents

	<u>Page</u>
List of Figures	v
List of Tables	vii
1. Introduction	1
2. Linearized Equations of Motion	2
3. Linear Aerodynamics	6
4. Three-Component Motion in a Vacuum	11
5. Flare-Stabilized Rod	14
6. Finned Missile	16
7. Beam Damping	17
8. Bent Missile	18
9. Quadratic Roll Equation	21
10. Summary	24
11. References	41
Appendix A: Aerodynamic Properties of a Finned Missile	43
Appendix B: Internal Beam-Supported Mass	49
List of Symbols	55
Distribution List	59
Report Documentation Page	63

INTENTIONALLY LEFT BLANK.

List of Figures

<u>Figure</u>	<u>Page</u>
1. X-Y Coordinates for Three-Component Projectile	25
2. X-Z Coordinates for Three-Component Projectile	25
3. $\omega_1/\hat{\omega}$ vs. r_m	26
4(a). $\dot{\phi}_1/\omega_R$ vs. σ for Flare-Stabilized Rod.....	26
4(b). $ E_2/\xi $ and $ E_3/\xi $ vs. σ for Flare-Stabilized Rod.....	27
5. $\dot{\phi}_1/\omega_R$ vs. σ for Finned Missile.....	27
6. $ \Gamma_j/\xi $ vs. σ ($j = 2, 3$) for Finned Missile	28
7. $\dot{\phi}_3/\omega_R$ and $\dot{\phi}_5/\omega_R$ vs. σ for Finned Missile.....	28
8. λ_1 vs. p/ω_R for $\sigma = 5$; $k_2 = k_3 = 0, 0.05, \text{ and } 0.10$	29
9. λ_2 vs. p/ω_R for $\sigma = 5$; $k_2 = k_3 = 0, 0.05, \text{ and } 0.10$	29
10. λ_1 vs. σ for $p = 2.3\omega_R$; $k_2 = k_3 = 0, 0.05, \text{ and } 0.10$	30
11. Scaled Zero Spin Trim Angle $ s_{10} / s_{10R} $ vs. σ	30
12(a). $ s_1/s_{10} $ vs. p/ω_R for $\sigma = 5$	31
12(b). $ s_3/s_{10} $ vs. p/ω_R for $\sigma = 5$	31
12(c). $ s_5/s_{10} $ vs. p/ω_R for $\sigma = 5$	32
13. $f_i\omega_R^{-1}$ vs. p/ω_R for Bent Missile With $\sigma = 5$; $i = 1, 2$	32
14. p/ω_R vs. Time for Bent Missile With $\sigma = 5$	33

<u>Figure</u>	<u>Page</u>
A-1. Sketch of a Hypersonic Missile	45
B-1. λ_1 vs. $\hat{\omega}_3 / \dot{\phi}_{1R}$	52
B-2. λ_2 vs. $\hat{\omega}_3 / \dot{\phi}_{2R}$	53
B-3. $ \xi_T $ and $ E_{3r} $ vs. $p / \hat{\omega}_3$	53

List of Tables

<u>Table</u>	<u>Page</u>
1. Nonaerodynamic Matrix Elements	34
2. Aerodynamic Matrix Elements	35
3. Flare-Stabilized Rod Parameters.....	37
4. Finned Missile Parameters.....	38
5. Bent Missile Terms	39
6. s_j/s_{10} for Resonant Spins, $\sigma = 5$	39
B-1. Parameters for Spinning Projectile With Interior Beam-Mounted Mass.....	52

INTENTIONALLY LEFT BLANK.

1. Introduction

The linear flight mechanics of spinning projectiles was first developed after World War I and later extended after World War II [1-4]. These results were reformulated by Platus [5] in missile-fixed coordinates for reentry vehicles. Thus, the linear flight mechanics of symmetric projectiles, including finned missiles, is well established. Nonlinear flight mechanics, as well as the effect of liquid payloads, have also been extensively addressed [4, 6, 7].

Recently, with the development of long-finned anti-armor projectiles and long flare-stabilized reentry vehicles, the effects of aero-elasticity have become a matter of possible concern for designers. In 1992, Platus [8] developed a simple theory for elastically deforming missiles. This theory showed significant decreases in pitching frequency when the smallest bending frequency was less than four times the pitching frequency. He also showed that linear beam damping could actually make the missile dynamically unstable when the spin was greater than the pitching frequency.

Platus assumed that the elastic missile oscillated in the modal waveform of a nonspinning, free-free beam. For uniform mass distribution, the waveform is symmetric with equal deflections at each end. The aerodynamic loads on a finned missile, however, are quite different at the nose and the tail, and this may not be a good assumption. Moreover, it would be desirable to predict the resonant response induced by mass or aerodynamic asymmetries at aerodynamic or elastic frequencies. The response of a spin-stabilized body of revolution to the motion of an interior elastic beam-mounted mass was studied, and beam damping destabilized the shell [9, 10]. Since all shells have spin rates that exceed their pitching frequencies, this is in agreement with Platus' result.

In this report, the beam theory [9, 10] was used to construct a simple model of an elastic projectile acted on by two significant aerodynamic loads. The complicated elastic projectile was replaced by three rigid projectile components connected by two massless cantilevered beams. Next, this three-body model was used to yield good predictions of the frequency of the motion of

a uniform free-free beam flying in a vacuum. With the inclusion of aerodynamic terms, the frequencies and damping of the angular motion of a symmetric elastic missile can be estimated from a 5×5 determinant.

Beam damping should be based on derivatives in a missile-fixed coordinate system. Thus, beam damping has no effect on the trim motion, which is constant in these coordinates. Resonance frequencies, however, will decrease as the ratio of elastic frequency to rigid-body pitching frequency decreases. Beam damping can adversely affect the damping of transients. Finally, the effect of permanent deformations were considered (i.e., the case of a "bent" missile). These deformations affect the size of resonant trim and introduce the possibility of spin-pitch lock-in [11].

2. Linearized Equations of Motion

The actual projectile is approximated by a homogenous cylinder of fineness ratio, L , and mass, m , divided into three segments with fineness ratios, L_j , and masses, m_j . A fixed-plane coordinate system, which pitches and yaws with the center segment (component 1) and has an origin located at the center of mass (cm) of the center segment, is shown in Figures 1 and 2. (Fixed plane coordinates roll so that the Z axis is always in the X_e - Z_e plane.) Its orientation with respect to earth fixed axes (ψ, θ) and the velocity vector (β, α) are also shown in the figures.

For $j = 2$ and 3 , let (X_j, Y_j, Z_j) be the location of the cm of component j with respect to the cm of component 1, and let $(\Gamma_{yj}, \Gamma_{zj})$ be the inclination of the forward body ($j = 2$) and of the rear body ($j = 3$), as shown in Figures 1 and 2.

Next, it is assumed that the fore and aft components are elastically connected to the center component by two massless cantilever beams of lengths a and b and stiffness $(EI)_j$. The moment and force exerted on these components by these beams can be computed from simple beam theory [10]. For motion in the x - y plane,

$$\hat{F}_{yj} = b_{1j}Y_j + b_{2j}\Gamma_{yj}, \quad (1)$$

and

$$\hat{M}_{zj} = b_{2j}Y_j + b_{3j}\Gamma_{yj}, \quad (2)$$

where $b_{12} = -(12/a^3)(EI)_2$, $b_{13} = -(12/b^3)(EI)_3$, $b_{22} = (6/a^2)(EI)_2$, $b_{23} = -(6/b^2)(EI)_3$, $b_{32} = -(4/a)(EI)_2$, and $b_{33} = -(4/b)(EI)_3$.

Similar relations apply for \hat{F}_{zj} and \hat{M}_{yj} .

For the dynamics analysis, a coordinate system with its origin at the center of mass of the complete projectile is much more convenient. Throughout this report, complex quantities are used to describe the lateral motion of the three components. Their lateral locations are specified by the dimensionless complex variables E_j , and their axial location by the dimensionless variable x_j . Both the lateral and axial locations are with respect to the projectile cm.

$$E_j - E_1 = (Y_j + iZ_j)/d; \quad E_1 = -(m_2E_2 + m_3E_3)/m_1; \quad (3)$$

$$x_j = (X_j/d) + x_1; \quad \text{and} \quad x_1 = -(m_2X_2 + m_3X_3)/md. \quad (4)$$

The complex beam forces and moments exerted on the forward and aft components are

$$\hat{F}_j = b_{1j}(E_j - E_1)d + b_{2j}\Gamma_j, \quad (5)$$

and

$$\hat{M}_j = i[b_{2j}(E_j - E_1)d + b_{3j}\Gamma_j], \quad (6)$$

where $\Gamma_j = \Gamma_{yj} + i\Gamma_{zj}$.

The velocity vector of the j-component is (v_{xj}, v_{yj}, v_{zj}) , and the complex transverse velocity is

$$v_{yj} + iv_{zj} = \dot{E}_j d + V\xi - ix_j Qd, \quad (7)$$

where $\xi = \beta + i\alpha$, the complex angle of attack,

$Q = \dot{\theta} + i\dot{\psi}$, the complex transverse angular velocity, and

$V \cong v_{xj}$ is the magnitude of the projectile's velocity.

The transverse components of the equations of motion for each component's center of mass can provide differential equations for the E_j 's,

$$m_j [\ddot{E}_j d + \dot{V}(\dot{\xi} - iQ) + \dot{V}\xi - ix_j \dot{Q}d] = \hat{F}_j + F_j, \quad (8)$$

where F_j is the transverse aerodynamic force acting on the j component. The axial beam forces, \hat{F}_{xj} , are determined by the requirement that each component has the same axial velocity,

$$m_j \dot{V} \cong m_j v_{xj} = \hat{F}_{xj} + F_{xj}, \quad (9)$$

where F_{xj} is the axial aerodynamic force acting on the j component.

The angular momentum of each component, \vec{H}_j , can be simply expressed in fixed-plane coordinates that pitch and yaw with that component,

$$\vec{H}_j = (I_{xj} p, I_{yj} (\dot{\theta} - \dot{\Gamma}_{zj}), I_{yj} (\dot{\psi} + \dot{\Gamma}_{yj})), \quad (10)$$

where $\Gamma_1 = 0$.

After differentiating each angular momentum vector, three differential equations can be written for the two Γ_j 's, and Q from the transverse components,

$$I_{ij}(\dot{Q} + i\ddot{\Gamma}_j) - ipI_{xj}(Q + i\dot{\Gamma}_j) = \hat{M}_j + M_j, \quad (11)$$

where M_j is the transverse aerodynamic moment acting on the j component.

The forces exerted on the center component by the other components are the negatives of the beam forces, and the moment exerted on the center component can be computed from the negatives of the beam forces and moments.

$$\hat{F}_1 = -\hat{F}_2 - \hat{F}_3; \hat{F}_{x1} = -\hat{F}_{x2} - \hat{F}_{x3}, \quad (12)$$

and

$$\hat{M}_1 = -\hat{M}_2 - \hat{M}_3 - i[(x_2 - x_1)\hat{F}_2 + (x_3 - x_1)\hat{F}_3 + \hat{F}_{x2}(E_2 - E_1) + \hat{F}_{x3}(E_3 - E_1)]d. \quad (13)$$

The sum of equations 9 yields the usual drag equation,

$$m\dot{V} = \sum_{j=1}^3 F_{xj}. \quad (14)$$

Equations 8 can be added to eliminate the beam forces to provide a simple relation between Q and ξ ,

$$V(\dot{\xi} - iQ) = \sum_{j=1}^3 [F_j - \xi F_{xj}]. \quad (15)$$

Equations 8 is now multiplied by $i(x_j - x_1)d$, equations 9 multiplied by $i(E_j - E_1)d$, and all are added to the sum of equation 11 to eliminate the beam forces and moments. The resulting differential equation for Q is simplified to

$$I_t \dot{Q} - ipI_x Q = \sum_{j=2}^3 \left[m_j (x_j - x_1) \ddot{E}_j d^2 + I_{tj} \ddot{\Gamma}_j - ipI_{xj} \dot{\Gamma}_j \right] + \sum_{j=1}^3 \left[M_j + i(x_j F_j + F_{xj} E_j) d \right], \quad (16)$$

where

$$I_t = I_{t1} + I_{t2} + I_{t3} + \left[m_1 (x_1)^2 + m_2 (x_2)^2 + m_3 (x_3)^2 \right] d^2 \text{ and} \\ I_x = I_{x1} + I_{x2} + I_{x3}.$$

3. Linear Aerodynamics

The linear aerodynamic forces and moments acting on the three bodies have the following forms in terms of the angle of attack at each body,

$$F_{xj} = -g_1 c_{Dj}, \quad (17)$$

$$F_{yj} + iF_{zj} = -g_1 \left[\left[c_{1j} + i(pd/V)c_{1j}^* \right] \xi_j + c_{2j} \dot{\xi}_j d/V \right], \quad (18)$$

and

$$M_{yj} + iM_{zj} = -ig_1 d \left[\left[c_{3j} + i(pd/V)c_{3j}^* \right] \xi_j + c_{4j} \dot{\xi}_j d/V \right], \quad (19)$$

where $g_1 = \rho S V^2 / 2$.

The Magnus force and moment coefficients (c_{1j}^*, c_{3j}^*) are usually neglected for slowly spinning finned missiles, but must be retained for spin-stabilized bodies of revolution. The local angles of attack at the three components are determined by their location, inclinations, and motion, *

$$\xi_j = \xi - \dot{\xi} x_j d / V - \Gamma_j + \dot{E}_j d / V. \quad (20)$$

The transverse aerodynamic force on the rigid projectile is obtained by adding the three equations 18 and using equation 20 for $\Gamma_j = \dot{E}_j = 0$.

$$F_{yR} + iF_{zR} = -g_1 \left[(c_1 + i(pd/V)c_1^*) \xi + c_2 (\dot{\xi} d / V) \right], \text{ and} \quad (21)$$

$$C_{N\alpha} = c_l = \sum_1^3 c_{lj},$$

$$\text{where } C_{Np\alpha} = c_l^* = \sum_1^3 c_{lj}^* \text{ and } C_{Nq} + C_{N\dot{\alpha}} = c_2 = \sum_1^3 [c_{2j} - x_j c_{lj}].$$

Similarly, the transverse aerodynamic moment for the rigid projectile is obtained by adding the sum of $ix_j d$ times each of equations 18 to the sum of equation 19 and again using equation 20.

$$M_{yR} + iM_{zR} = -ig_1 d \left[(c_3 + i(pd/V)c_3^*) \xi + c_4 (\dot{\xi} d / V) \right], \text{ and } C_{M\alpha} = c_3 = \sum_1^3 [c_{3j} + x_j c_{1j}], \quad (22)$$

* In reference 8, the relation similar to equation 20 erroneously uses the missile-fixed derivative of E_j , and not the derivative in a nonspinning coordinate system.

where $C_{M\dot{p}\alpha} = c_3^* = \sum_1^3 [c_{3j}^* + x_j c_{1j}^*]$ and $C_{Mq} + C_{M\dot{\alpha}} = c_4 = \sum_1^3 [c_{4j} + x_j (c_{2j} - c_{3j}) - (x_j)^2 c_{1j}]$.

From equations 14 and 17, the familiar form of the drag equation is written

$$m\dot{V} = -g_1 C_D, \quad (23)$$

where $C_D = c_{D1} + c_{D2} + c_{D3}$.

For the aerodynamic force, equations 17–19 can be inserted in equation 14, and the small effects of the Magnus force, the damping force, and the center body lift on the trajectory can be neglected ($c_{1j}^* = c_{2j} = c_{11} = 0$).

$$mV(\dot{\xi} - iQ) = -g_1 \left[C_{L\alpha} \xi - c_{12} (\Gamma_2 - \dot{E}_2 d/V) - c_{13} (\Gamma_3 - \dot{E}_3 d/V) \right], \quad (24)$$

where $C_{L\alpha} = C_{N\alpha} - C_D$.

Equations 8 and 11 for $j = 2, 3$ and equations 15 and 16 are six differential equations in six variables— ξ , Q , E_2 , Γ_2 , E_3 , and Γ_3 . If the aerodynamic forces and moments of equations 17–19 are inserted and Q is eliminated by equation 24, a set of five equations in five variables results, as in

$$\sum_{m=1}^5 [R_{nm} \ddot{z}_m + (S_{nm} + ipS_{nm}^*) \dot{z}_m + (T_{nm} + ipT_{nm}^*) z_m] = 0; \text{ and } n=1, 2, 3, 4, 5, \quad (25)$$

where $(z_1, z_2, z_3, z_4, z_5) = (\xi, E_2, \Gamma_2, E_3, \Gamma_3)$.

R_{nm} and S_{nm}^* are primarily dynamics terms involving various masses and moments of inertia. The aerodynamic contributions to these terms are quite small and will be neglected. T_{nm} contains combinations of beam elastic terms and aerodynamic terms, while S_{nm} and T_{nm}^* are combinations of beam damping terms and aerodynamic terms. In equation 25,

$$T_{nm} = \hat{T}_{nm} + g_1 \tilde{T}_{nm},$$

$$S_{nm} = \hat{S}_{nm} + (g_1 d/V) \tilde{S}_{nm}, \text{ and} \quad (26)$$

$$T_{nm}^* = \hat{T}_{nm}^* + (g_1 d/V) \tilde{T}_{nm}^*.$$

Twenty of the dynamics terms, twelve of the elastic terms, and eight of the beam damping terms are nonzero; these forty terms are given in Table 1. The forty-six nonzero aerodynamic terms are given in Table 2.

A general solution of equation 25 can be expressed as the sum of ten modal functions of the form

$$z_m = z_{mk} e^{A_k t} \quad \text{and} \quad A = A_k, \quad k = 1 \text{ to } 10. \quad (27)$$

When a function of this type is substituted into equation 25, the final result can be written in the form of five linear homogenous equations in the constants z_{mk} . These equations are specified by a 5×5 matrix (u_{nm}) which is a function of A .

$$\sum_{m=1}^5 u_{nm} z_{mk} = 0 \quad \text{and} \quad n = 1, 2, 3, 4, 5, \quad (28)$$

where $u_{nm} = A_k^2 R_{nm} + A_k (S_{nm} + ip S_{nm}^*) + T_{nm} + ip T_{nm}^*$.

The ten values of A_k are the roots of

$$\det u_{nm} = 0. \quad (29)$$

For $z_{1k} \neq 0$, the corresponding values of the z_{mk} 's for each of the ten modes can be determined from the solution of a fourth-order inhomogeneous linear system,

$$\sum_{m=1}^4 w_{nm} y_{mk} = w_n \quad \text{and } n = 1, 2, 3, 4, \quad (30)$$

where $w_{nm} = u_{(n+1)(m+1)}$,

$y_{mk} = z_{(m+1)k} / z_{1k}$, and

$w_n = -u_{(n+1)1}$.

Equation 29 can be solved in general by a simple trial-and-error Newton's quadratic formula. The first of the five modal equations is

$$\begin{aligned} I_1 A^2 + (S_{11} - ipI_x)A + T_{11} + ipT_{11}^* &= [m_2(x_2 - x_1)d^2 A^2 - S_{12}A - T_{12}]y_1 \\ &+ [(I_{12}A - ipI_{x2})A - S_{13}A - T_{13} - ipT_{13}^*]y_2 \\ &+ [m_3(x_3 - x_1)d^2 A^2 - S_{14}A - T_{14}]y_3 \\ &+ [(I_{13}A - ipI_{x3})A - S_{15}A - T_{15} - ipT_{15}^*]y_4. \end{aligned} \quad (31)$$

(The k subscript has been omitted from equation 31 for simplicity). The rigid projectile frequencies and damping rates can be computed from equation 31 when the y_j 's are zero. Very good approximations [4] for the frequencies are

$$\phi_{kR} = \left[pI_x \pm \sqrt{(pI_x)^2 + 4I_1 T_{11}} \right] / 2I_1 \cong \pm \omega_R + (1 \pm pI_x / 4I_1 \omega_R) pI_x / 2I_1, \text{ and } k = 1, 2, \quad (32)$$

where $\omega_R = \sqrt{T_{11}/I_t}$ is the rigid projectile zero-spin frequency. Exact relations for the damping rates are

$$\lambda_{kR} = -(S_{11}\dot{\phi}_{kR} + pT_{11}^*) / (2\dot{\phi}_{kR}I_t - pI_x). \quad (33)$$

The magnitude of y_{2k} specifies the relative size of the angular motion of the fore component with respect to the projectile angular motion for mode k , while the magnitude of y_{4k} specifies the angular motion of the rear component for that mode. For example, the argument of y_{4k} determines whether the fins of an elastic missile are more or less effective than those on a rigid projectile. Usually, the phase angle is near zero and they are less effective.

4. Three-Component Motion in a Vacuum

A nonspinning projectile with identical components 2 and 3 and identical connecting beams is now considered. For this case, all parameters for components 2 and 3 are equal, except for $x_2 = -x_3$ and $b_{22} = -b_{23}$. For motion in a vacuum, $g_I = 0$ and the aerodynamic terms vanish. The five equations of motion become

$$\left[I_t z_{1k} - m_2 x_2 (z_{2k} - z_{4k}) d^2 - I_{t2} (z_{3k} + z_{5k}) \right] A^2 = 0, \quad (34)$$

$$-m_2 x_2 A^2 z_{1k} + [m_2 A^2 - b_{12}(1+r_m)] z_{2k} - (b_{22}/d) z_{3k} - b_{12} r_m z_{4k} = 0, \quad (35)$$

$$I_{t2} A^2 z_{1k} + b_{22} d(1+r_m) z_{2k} + (-I_{t2} A^2 + b_{32}) z_{3k} + b_{22} d r_m z_{4k} = 0, \quad (36)$$

$$m_2 x_2 A^2 z_{1k} - b_{12} r_m z_{2k} + [m_2 A^2 - b_{12}(1+r_m)] z_{4k} + (b_{22}/d) z_{5k} = 0, \quad (37)$$

and

$$I_{12}A^2 z_{1k} - b_{22}dr_m z_{2k} - b_{22}d(1+r_m)z_{4k} + (-I_{12}A^2 + b_{32})z_{5k} = 0, \quad (38)$$

where $r_m = m_2/m_1$.

Equation 34 indicates that zero is a double root ($A_1 = A_2 = 0$). If modal functions are considered for which $z_{2k} = z_{4k}$ and $z_{3k} = -z_{5k}$, z_{1k} is zero, and equations 37 and 38 are identical to equations 35 and 36. Thus, four more roots are the solutions of a quadratic in A^2 , as in

$$[m_2A^2 - b_{12}(m/m_1)][I_{12}A^2 - b_{32}] - (b_{22})^2(m/m_1) = 0. \quad (39)$$

For small I_{12} ,

$$A_{3,4} = \pm i\sqrt{3mEI/(m_1m_2a^3)}, \text{ and } A_{7,8} = \pm 2i\sqrt{EI/(I_{12}a)}. \quad (40)$$

The third and fourth roots are particularly interesting. Planar motion occurs when $z_{23} = z_{24}$. The sum of the modal functions for E_j is

$$E_2 = E_3 = 2z_{23} \cos \omega t, \quad (41)$$

where $\hat{\omega} = I\{A_3\}$ and $I\{a+ib\} = b$.

This in-phase symmetric motion of the fore and aft components is quite similar to that for the classical free-free beam vibration. Geradin and Rixen [12] give the theoretical frequency for two lower free-free vibrations as

$$\omega_k = \lambda_k^2 \sqrt{EI/(mL^3 d^3)}, \quad (42)$$

where $\lambda_1 = 4.730$, $\lambda_2 = 7.853$.

If the length of the beam is assured to be the distance between the cm's of the center component and the forward component,

$$a = x_2 d = (L/2)(1 + r_m)/(1 + 2r_m), \quad (43)$$

and

$$\omega_1/\hat{\omega} = (4.566)\sqrt{r_m(1+r_m)^3/(1+2r_m)^5}. \quad (44)$$

$\omega_1/\hat{\omega}$ is plotted vs. the mass ratio r_m in Figure 3, and the three-body approximation is quite good for fore and aft components which are one half the mass of the center component or are each 25% of the total mass. In the numerical examples of this report, each end component is specified to have one quarter of the total mass.

The remaining four roots can be obtained by assuming an antisymmetric oscillation of the end bodies (i.e., $z_{2k} = -z_{4k}$ and $z_{3k} = z_{5k}$). Equation 34 becomes

$$z_{1k} = \left[2m_2 x_2 d^2 z_{2k} + I_{t2} z_{3k} \right] / I_t, \quad (45)$$

and equations 37 and 38 reduce once again to equations 35 and 36. The last four roots are solutions of the following equation in A^2 :

$$\left[m_2 a_1 A^2 - b_{12} \right] \left[I_{t2} a_2 A^2 - b_{32} \right] - \left[2m_2 x_2 (I_{t2}/I_t) A^2 + b_{22} \right]^2 = 0, \quad (46)$$

where $a_1 = 1 - 2m_2(x_2)^2 d^2 / I_t$ and $a_2 = 1 - 2I_{t2} / I_t$.

For small I_{t2} ,

$$A_{5,6} = \pm i \sqrt{3EI/(m_2 a_1 a^3)}, \quad \text{and} \quad A_{9,10} = \pm 2i \sqrt{EI/(I_{t2} a)}. \quad (47)$$

The ninth and tenth roots are approximately equal to the seventh and eight roots. These roots correspond to very high frequencies and will not be considered in the remainder of this report.

If I_t is assumed to be the value for a slender uniform cylinder of length L , I_t is $mL^2/12$.

The ratio of $A_{5,6}$ to $A_{3,4}$ can be derived from equations 40, 43, and 47, as in

$$A_{5,6} = A_{3,4} (1 + 2r_m) / \sqrt{1 + 2r_m^3}. \quad (48)$$

Roots five and six represent a pitching motion of the center component, combined with an opposing oscillation of the fore and aft components. For $r_m = 0.5$, this pitching antisymmetric motion is 80% faster than the free-free in-phase oscillation that was considered earlier. The second free-free oscillation is antisymmetric, but is 180% greater than the first. Thus, the three-body theory qualitatively describes this oscillation, but predicts its frequency very poorly.

5. Flare-Stabilized Rod

Platus [8] first applied his theory to a 5-ft-long rod stabilized by a very light 1.5-ft-long flare with a base diameter of 0.8 ft. Since he neglected the very small normal force associated with the nose, this missile has a very simple normal force distribution of

$$\frac{dC_{N\alpha}}{dx} = -1.138(x + 1.25) \quad \text{and} \quad -3.12 \leq x \leq -1.25. \quad (49)$$

The displacement oscillations of a free-free uniform beam can be described by the following sum of eigenfunctions:

$$\delta(x,t) = \sum \hat{\delta}_K \Psi_K(x) \exp(i\omega_K t), \text{ and } -L/2 \leq x \leq L/2. \quad (50)$$

The $\hat{\delta}_K$'s are constants determined by initial conditions. The first two eigenfrequencies, ω_K , were given by equation 42, and the corresponding eigenfunctions are

$$\Psi_1(x) = \cosh(\lambda_1 x/L) - \eta_1 \cos(\lambda_1 x/L), \text{ and } \Psi_2(x) = \sinh(\lambda_2 x/L) - \eta_2 \sin(\lambda_2 x/L), \quad (51)$$

where $\eta_K = 7.527, 35.975$.

The other pairs of eigenfunctions for K greater than 2 have the same form as equation 51, with larger values of λ_K, η_K .

The linear motion of an elastic missile with distributed aerodynamic loads can be expressed as a sum of periodic functions. Their frequencies are related to the aerodynamic frequencies of the rigid projectile and the free oscillation frequencies of the elastic projectile. Platus assumed that each of the periodic components had the form

$$\delta_k(x,i) = \left[\sum_K \hat{\delta}_{kK} \Psi_K(x) \right] \exp(A_k t) \text{ and } I\{A_k\} = \dot{\phi}_k. \quad (52)$$

Although the first three eigenfunctions were used to compute the motion of the flare-stabilized rod, the second and third eigenfunctions had very little effect on the low frequency motion. The first eigenfunction gave the following expression for the lowest four frequencies:

$$\left[I_t (\dot{\phi}_k)^2 - p I_x \dot{\phi}_j - T_{11} \right] \left[(\dot{\phi}_k)^2 - \omega_1^2 + I_6/M_1 \right] = I_1 I_4 / M_1. \quad (53)$$

The ratio of the displacement at position x and the angle of attack for the k -th frequency is

$$\delta_k(x)/\xi = [\Psi_1(x)][I_1/M_1][(\dot{\phi}_k)^2 - \omega_1^2 + I_6/I_1]^{-1}. \quad (54)$$

Table 3 provides the appropriate parameters, including Platus's integrals I_1, I_4, I_6 , and M_1 . The parameters for the three-body theory are given for $m_2 = m_3 = m_1/2$.

The ratio of the three-body elastic frequency, $\hat{\omega}$, to the rigid-body zero-spin pitch frequency, ω_R , is a good measure of the effect of elasticity on the projectile's aerodynamic frequencies and damping rates. This ratio, $\hat{\omega}/\omega_R$, is denoted by σ and is usually greater than 5. When it is less than 5, a large effect on the aerodynamic motion is expected. By varying EI , $\dot{\phi}_1/\omega_R$ can be computed as a function of σ . The result is plotted as Figure 4a and compared with the three-body theory. In Figure 4b, the two deflection magnitudes, $|E_j/\xi|$, of the three-body theory are also plotted against σ , and they are compared with the corresponding deflection magnitude, $[\delta_1(3L/8)]/\xi$, of the Platus [8] theory. (The three-body deflections are given by y_{11} and y_{31} in equation 30.)

These figures show similar behavior for the two theories. The three-body theory predicts a much slower decrease in $\dot{\phi}_1$, with decreasing σ and a displacement of the aft component that is twice that of the forward component. For $\sigma = 2$, the flare angle of attack is reduced by 40%, thereby reducing the frequency by 23%.

6. Finned Missile

The implications of this aeroelastic theory can best be seen by considering a particular hypersonic finned projectile with a fineness ratio of 20 flying at 6,000 ft/s. This projectile has a body diameter of 0.35 ft, and its forward and rear segments are each 25% of the total length; this is slightly less than the optimum length of 27%. The various aerodynamic coefficients are computed from an assumed force distribution (see Appendix A). All necessary parameters are

listed in Table 4. For zero spin, the rigid body frequency ω_r is 8.52 Hz, and the rigid body damping rate is -2.4 s^{-1} . For $\sigma = 8$, the three-body symmetric beam frequency ω is 69.0 Hz, and the elastic projectile frequency is 8.06 Hz (i.e., 6.5% less than the rigid body frequency).

The equations derived in section 3 can now be used to calculate $\dot{\phi}_1/\omega_r$ as a function of σ between 1.0 and 10.0. The result is plotted in Figure 5, while the magnitudes of Γ_2/ξ and Γ_3/ξ are plotted in Figure 6. For $\sigma = 4$, the effective angle of attack of the fins has been reduced by 30%, and the adverse angle of the nose increased by 35%, thereby reducing the projectile frequency by 45%. The large nose deflection with its increased destabilizing moment has a large effect on the projectile frequency, which did not appear for the flare-stabilized missile. In Figure 7, the elastic frequencies $\dot{\phi}_3/\omega_r$ and $\dot{\phi}_5/\omega_r$ are plotted against σ . The frequency of the antisymmetric pitching oscillation, $\dot{\phi}_5$, is seen to be approximately twice $\dot{\phi}_3$, the symmetric oscillation.

7. Beam Damping

Beam damping is a very complicated process that will be approximated by a simple linear proportionality with the displacement velocity. This velocity must be computed in a coordinate system spinning with the beam. Thus, the damping force exerted by each beam is assumed to have the form:

$$\left(\hat{F}_{yj} + i\hat{F}_{zj}\right)_{damp} = -2k_j m_j \hat{\omega}_j e^{i\phi} \frac{d}{dt} \left[(E_j - E_1) e^{-i\phi} \right] = -2k_j m_j \hat{\omega}_j \left[\dot{E}_j - \dot{E}_1 - ip(E_j - E_1) \right], \text{ and}$$

$$\hat{\omega}_2 = \sqrt{3(EI)_2 / (m_1 m_2 \alpha^3)}, \quad (55)$$

where $\hat{\omega}_3 = \sqrt{3(EI)_3 / (m_1 m_3 b^3)}$ and $\dot{\phi} = p$.

The definition of k_j was selected so that $k_j = 1$ corresponds to the critical damping of a free-free beam. For example, the forward beam damping contribution to the first mode is

$$-2k_2 m_2 \hat{\omega}_2 [\lambda_1 + i(\dot{\phi} - p)] [(m_1 + m_2)z_{21} + m_3 z_{41}] / m_1.$$

Thus, beam damping is a strong function of spin and is essentially zero when spin is equal to the modal frequency. The beam damping terms are given in Table 1(c). In Figure 8, the finned missile's fast mode damping rate, λ_1 , is plotted vs. spin for $\sigma = 5$ and $k_2 = k_3 = 0, 0.05$, and 0.10 . Beam damping increases projectile damping when spin is less than the modal frequency and decreases projectile damping when it is greater than modal frequency. Figure 9 shows λ_2 , the second projectile damping rate, for the same parameters. For this mode, the coning motion is opposite to the spin, the frequency is approximately the negative of the first frequency, and beam damping always increases the damping of this mode. Finally, Figure 10 shows λ_1 vs. σ for spin of $2.3\omega_R$, and $k_2 = k_3 = 0, 0.05$, and 0.10 . For low values of σ , beam damping can actually cause projectile instability. Indeed, Chadwick and Murphy [9, 10] show that the beam damping of an internally mounted beam can destabilize a spinning shell (Appendix B).

8. Bent Missile

If the beam deflection is large enough, the maximum stress exceeds the yield limit, and the beams are permanently deformed or bent. All future elastic motion will be about this new bent shape. Thus, the component location variables E_j and Γ_j are no longer completely elastic, but consist of an elastic part and a permanently bent part that rotates with the projectile,

$$E_j = \hat{E}_j + E_{jB} e^{i\phi} \quad (56)$$

and

$$\Gamma_j = \hat{\Gamma}_j + \Gamma_{jB} e^{i\phi}, \quad (57)$$

where $\dot{\phi} = \dot{p}$ and $\hat{E}_j, \hat{\Gamma}_j$ vary elastically.

Both fore and aft components will have trim force and trim moment terms associated with Γ_{jB} and E_{jB} in equation 20. If the fins are deformed relative to the aft component, additional fin force and moment terms must be added for the rear component, as in

$$(F_{y3} + iF_{z3})_{fin} = g_1 c_{13} \Gamma_{3F} e^{i\phi} \quad (58)$$

and

$$(M_{y3} + M_{z3})_{fin} = i g_1 d c_{33} \Gamma_{3M} e^{i\phi}, \quad (59)$$

where Γ_{3F} and Γ_{3M} are measures of the deformation.

The equations of motion derived in section 3 should be modified by inserting the new variables of equations 56 and 57 in the dynamics and aerodynamics terms, adding the fin trim terms to the aerodynamic force and moment, and replacing E_j, Γ_j with $\hat{E}_j, \hat{\Gamma}_j$ in the elastic terms. The new set of five inhomogeneous differential equations contains terms multiplied by $\exp(i\phi)$, as in

$$\sum_{m=1}^5 [R_{nm} \ddot{z}_m + (S_{nm} + ipS_{nm}^*) \dot{z}_m + (T_{nm} + ipT_{nm}^*) z_m] = t_n \exp(i\phi) \text{ and } n = 1, 2, 3, 4, 5, \quad (60)$$

where $t_n = (p^2 - ip)t_{nD} + p^2 t_{nD}^* + g_1 t_{nA} + ip(g_1 d/V)t_{nA}^*$

$t_{nD}, t_{nD}^*, t_{nA}, t_{nA}^*$ are defined in Table 5. Equation 60 can be solved by the assumptions of constant spin and a solution with the following form:

$$(z_1, z_2, z_3, z_4, z_5) = (\xi_T, \hat{E}_{2T}, \hat{\Gamma}_{2T}, \hat{E}_{3T}, \hat{\Gamma}_{3T}) \exp(ipt) = (s_1, s_2, s_3, s_4, s_5) \exp(ipt). \quad (61)$$

The s_j 's are solutions of the following linear inhomogeneous system of equations:

$$\sum_{m=1}^5 t_{nm} s_m = t_n, \quad n = 1, 2, 3, 4, \text{ and } 5, \quad (62)$$

where $t_{nm} = -p^2(R_{nm} + S_{nm}^*) + ip(S_{nm} + T_{nm}^*) + T_{nm}$.

A simple bent version of the finned missile is considered. All of the bent parameters are taken to be zero, except for $E_{3B} = -.063$ and $\Gamma_{3B} = .020$. In Figure 11, the zero-spin trim angle, $|s_{10}|$, divided by its zero-spin rigid body value, $|s_{10R}|$, is plotted against σ . For $\sigma = 4$, the flexible missile has a trim angle twice that for a rigid missile, and this angle increases rapidly with decreasing σ . The magnitude of the trim motion is smaller than that for zero spin motion, except in the vicinity of the five resonant spins. For $\sigma = 5$, the maximum values of the trim motion parameters for spin near the three lower-resonant frequencies are given in Table 6, and s_j/s_{10} vs. spin is plotted in Figures 12(a)–12(c) for $j = 1, 3, 5$.

For spin near $0.7\omega_R$ and $4.9\omega_R$, the forward and aft components move in phase with each other while they are out of phase for spin near $9.7\omega_R$. This out-of-phase motion is similar to the fifth and sixth modes for vacuum flight. For resonant spins of $0.7\omega_R$ and $9.7\omega_R$, the aft component moves to reduce the effective angle of attack of the fins, but it actually increases the effective angle of attack for the intermediate spin of $4.9\omega_R$. The motion of the two end bodies does dominate the two elastic beam resonant frequencies.

9. Quadratic Roll Equation

Since the trim motion is large in a very small region near resonant spin, the trim motion of rigid spinning finned missiles is usually a minor concern for designers. Some missiles, however, can "lock in" at resonant spin for a range of initial conditions. A rigid missile with mass asymmetry and a trim aerodynamic force can lock in at resonant spin [11]. Quadratic terms in the missile's roll equation cause this; therefore, the quadratic version of roll equations must be derived for the three components.

Each component's roll equation is expressed with respect to that component's fixed plane X-axis,

$$I_{xj} \dot{p}_j = \hat{M}_{xj} + g_1 c_{\ell j} d. \quad (63)$$

If linearity is assumed, then

$$p_1 = p_2 = p_3 = p, \quad (64)$$

$$\hat{M}_{x1} = -\hat{M}_{x2} - \hat{M}_{x3}, \quad (65)$$

and

$$I_x \dot{p} = g_1 c_{\ell} d, \quad (66)$$

where $c_{\ell} = c_{\ell 1} + c_{\ell 2} + c_{\ell 3} = C_{\ell p} (p - p_{ss}) d / V$.

p_{ss} is the linear steady-state spin produced by either intentional cant of the fins or unintentional damage to the fins.

The exact relations for p_2 and p_3 depend on the requirement that they should be equal to the corresponding body's fixed-plane X-component of the central body's angular velocity,

$$p_j = p[1 - \gamma_j^2/2] + \dot{\theta} \Gamma_{yj} + \dot{\psi} \Gamma_{zj} = p + R\{(Q - p\Gamma_j/2)\bar{\Gamma}_j\}, \quad (67)$$

where $\gamma_j = |\Gamma_j|$,

$R\{a + ib\} = a$, and

\bar{z} is the complex conjugate of z .

Equation 65 can be replaced by a more exact expression for the roll moment exerted on the central body by the two beams; this replacement is

$$\begin{aligned} \hat{M}_{x1} = & -\hat{M}_{x2}[1 - \gamma_2^2/2] + R\{\hat{M}_2\bar{\Gamma}_2\} - \hat{M}_{x3}[1 - \gamma_3^2/2] + R\{\hat{M}_3\bar{\Gamma}_3\} \\ & - I\{\hat{F}_2(\bar{E}_2 - \bar{E}_1)d + \hat{F}_3(\bar{E}_3 - \bar{E}_1)d\}. \end{aligned} \quad (68)$$

Equations 63, 67, and 68 can be combined to give the nonlinear version of equation 66, resulting in equation 69.

$$[I_x - (I_{x2}\gamma_2^2 + I_{x3}\gamma_3^2)/2]\dot{p} = g_1 c_t d + R\{\hat{M}_2\bar{\Gamma}_2 + \hat{M}_3\bar{\Gamma}_3\} - I\{\hat{F}_2(\bar{E}_2 - \bar{E}_1)d + \hat{F}_3(\bar{E}_3 - \bar{E}_1)d\} - \dot{C}_0, \quad (69)$$

where $C_0 = \sum_2^3 I_{xj} R\{(Q - p\Gamma_j/2)\bar{\Gamma}_j\}$.

Equation 69 is the nonlinear spin equation and must be combined with equation 60 to describe the motion of a bent missile. Any study of the steady-state solutions would require the numerical integration of equations 60 and 69. The linear spin equation had a constant steady-state solution, and constant steady-state solutions for the nonlinear spin equation are possible. Indeed, the nonlinear spin equation for a rigid bent missile has only constant steady-state solutions [11]. For

constant spin, the trim motion given by equations 61 and 62 describe the steady-state transverse motion of an elastic missile. If the equations for trim motion are inserted in equation 69 and \dot{p} is taken to be zero, the appropriate equation for equilibrium spins can be written.

$$g_1 C_{\ell p} (p - p_{ss}) d^2 / V = -(M_x)_{nl}, \quad (70)$$

where $(M_x)_{nl} = R \{ \hat{M}_{2T} \bar{\Gamma}_{2T} + \hat{M}_{3T} \bar{\Gamma}_{3T} \} - I \{ \hat{F}_{2T} (\bar{E}_{2T} - \bar{E}_{1T}) d + \hat{F}_{3T} (\bar{E}_{3T} - \bar{E}_{1T}) d \}$.

The trim values of E_j and Γ_j are defined in Table 5(b). Two functions of spin, $f_1(p)$ and $f_2(p)$, are defined as

$$f_1(p) = -(M_x)_{nl} (g_1 C_{\ell p} d^2 / V)^{-1}, \quad \text{and} \quad f_2(p) = p - p_{ss}. \quad (71)$$

Equation 70 states that equilibrium spins are spins for which f_1 intersects f_2 . $f_1(p)$ is a function of spin, and except for near resonance spin, it is quite small; equilibrium spin must be near the design p_{ss} . Near resonance, however, $f_1(p)$ is large. Although p_{ss} could be quite far from resonance spin, a near resonance spin could satisfy equation 70 and be an equilibrium spin. If this equilibrium spin is a stable equilibrium, it would be a possible constant steady-state spin and therefore produce spin-yaw lock-in. Numerical integration of the differential equations of motion, equations 60 and 69, would determine the stability of the equilibrium spins.

In Figure 13, $f_1(p)$ for a nonlinear roll moment is computed from equation 71 for the bent missile, and the result is plotted against p/ω_R . The line $f_2(p)$ for the linear roll moment is also plotted for $p_{ss} = 7\omega_R$. The three intersections of the two curves are equilibrium spins. The effect of other values of p_{ss} can be determined by changing the p/ω_R intercept of the $f_2(p)$ line. This process shows that $0.7\omega_R$ could be an equilibrium spin when p_{ss} is between $0.7\omega_R$ and $3.1\omega_R$, and similar observations apply for $4.9\omega_R$.

The equations of motion for the bent missile case were integrated for $p_{ss} = 7\omega_R$ and $\dot{p}_0 = 4.9\omega_R, 5.2\omega_R$. The resulting spin history is plotted against time in Figure 14. For \dot{p}_0 greater than $5.2\omega_R$, the spin goes to a constant value near the linear prediction of p_{ss} . For \dot{p}_0 between 0 and $4.9\omega_R$, it goes to a value of $4.7\omega_R$ near the lowest elastic frequency. Figure 14 shows that the boundary value of \dot{p}_0 , which separates these different behaviors, is approximately $5.05\omega_R$. Thus, spin lock-in can occur for this elastic frequency.

10. Summary

- (1) The aero-elastic motion of a flexible projectile is approximated by three bodies connected by two massless elastic beams.
- (2) This three-component projectile theory gives excellent estimates of the first elastic frequency of a free-free uniform beam.
- (3) Two types of beam motion are simulated—the classical free-free symmetric motion and an out-of-phase antisymmetric flexing motion combined with pitching motion.
- (4) When the elastic frequency is less than eight times the aerodynamic rigid body pitch frequency, the fins move to reduce the stabilizing moment significantly, and the pitch frequency can be significantly reduced.
- (5) Moderate beam damping can cause dynamic instability when the spin is much greater than the pitch frequency.
- (6) The trim motion of a bent missile shows large resonant responses when the spin is near the lower three modal frequencies.
- (7) The quadratic roll equation shows that spin-yaw lock-in can occur for the lower elastic frequency.

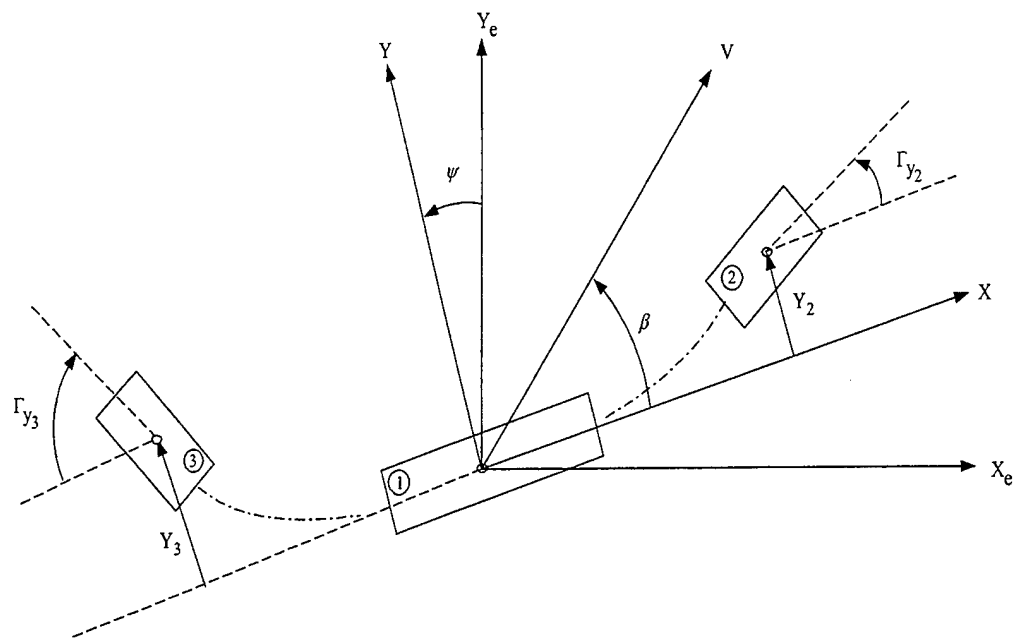


Figure 1. X-Y Coordinates for Three-Component Projectile (Every Variable Is Shown as Positive, Except Γ_{y3}).

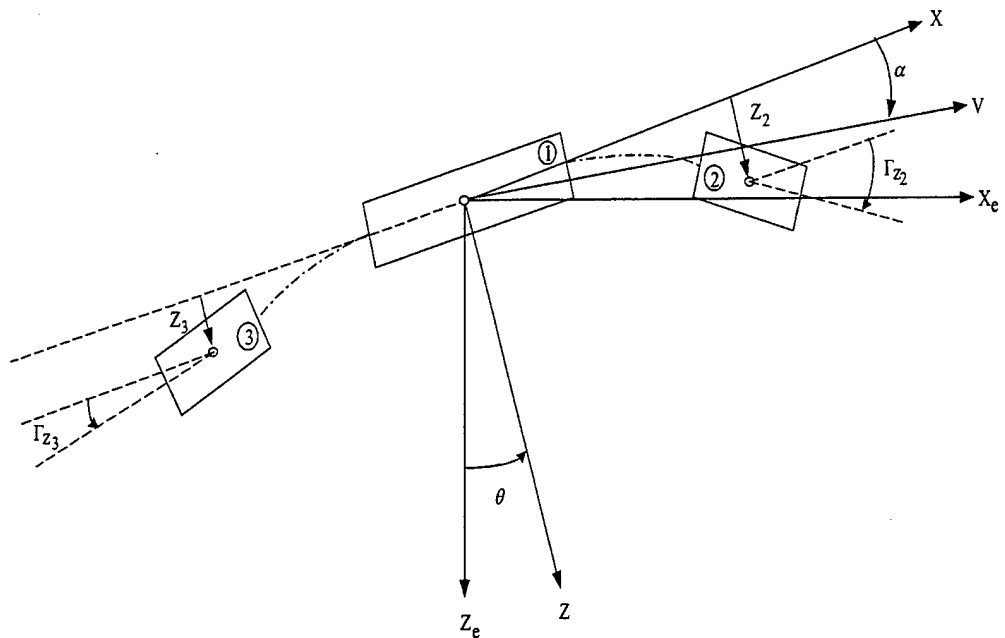


Figure 2. X-Z Coordinates for Three-Component Projectile (Every Variable Is Shown as Positive, Except Γ_{z3}).

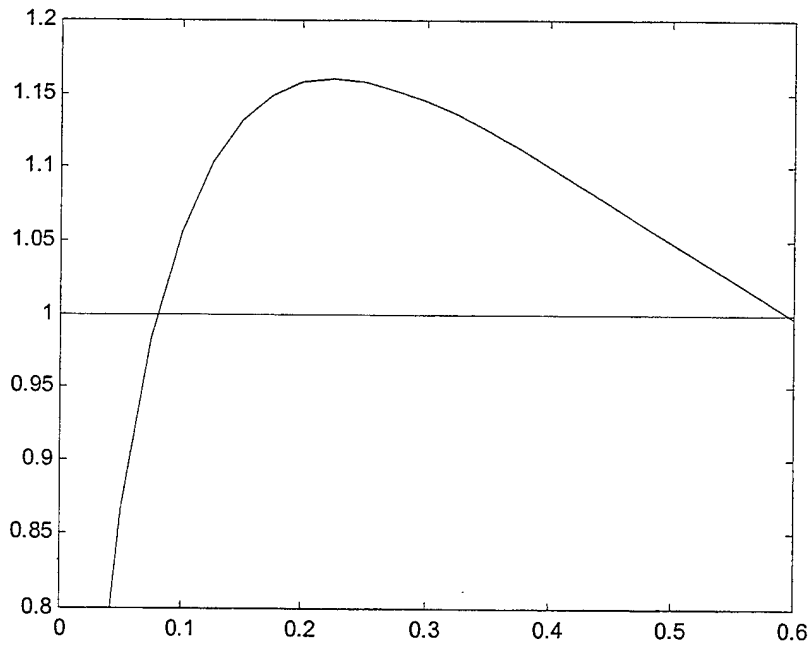


Figure 3. $\omega_1/\hat{\omega}$ vs. r_m .

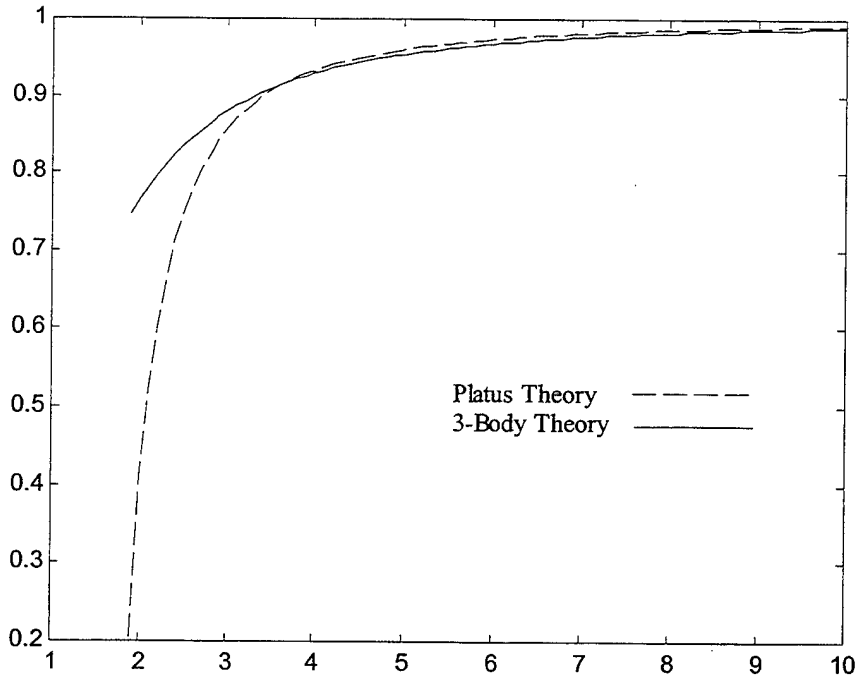


Figure 4(a). $\dot{\phi}_1/\omega_R$ vs. σ for Flare-Stabilized Rod.

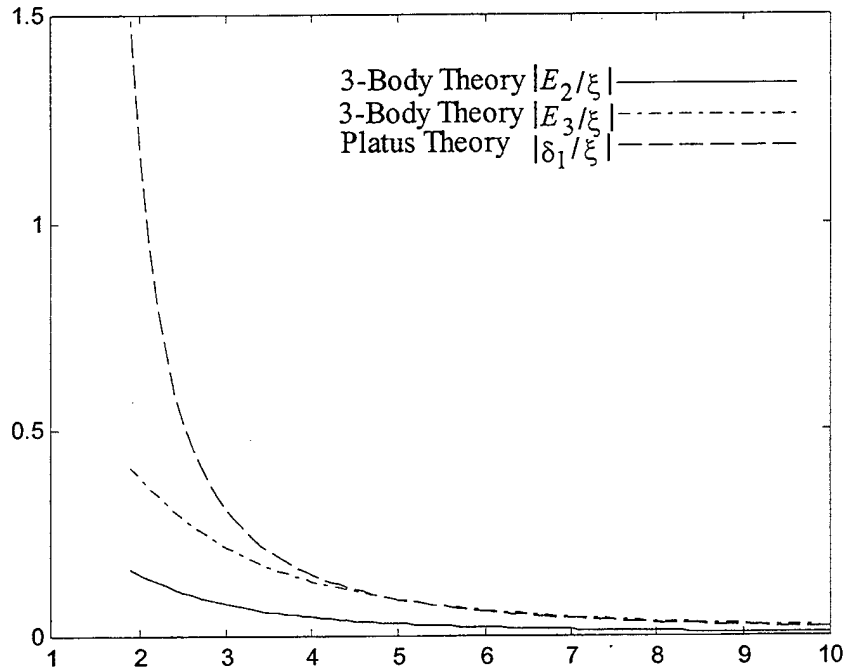


Figure 4(b). $|E_2/\xi|$ and $|E_3/\xi|$ vs. σ for Flare-Stabilized Rod.

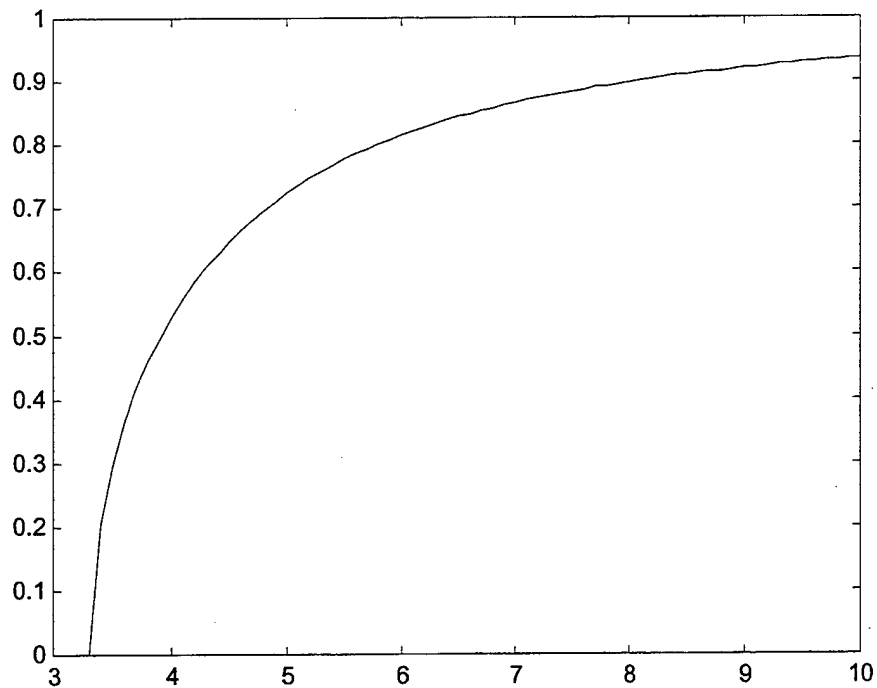


Figure 5. $\dot{\phi}_1/\omega_R$ vs. σ for Finned Missile.

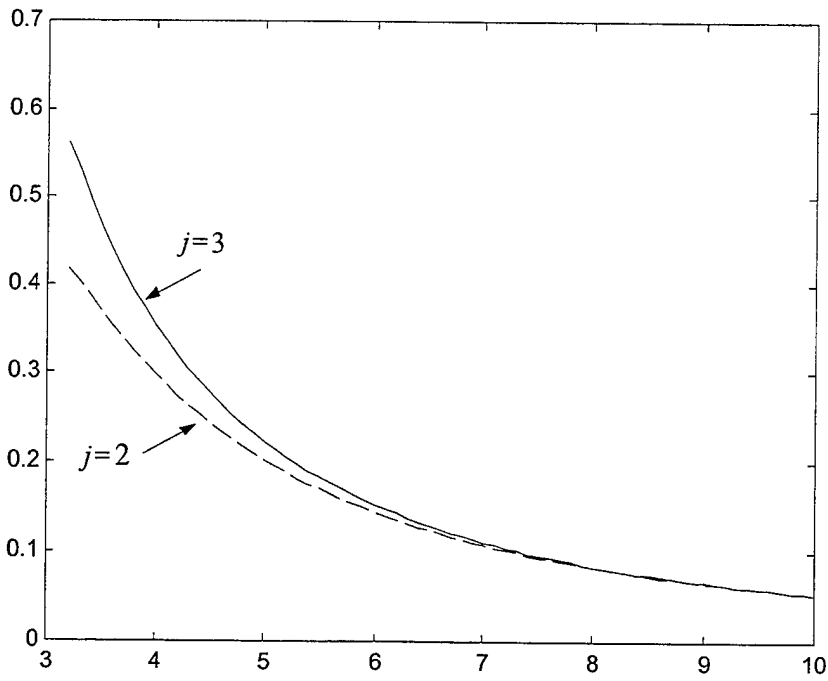


Figure 6. $|\Gamma_j/\xi|$ vs. σ ($j = 2, 3$) for Finned Missile.

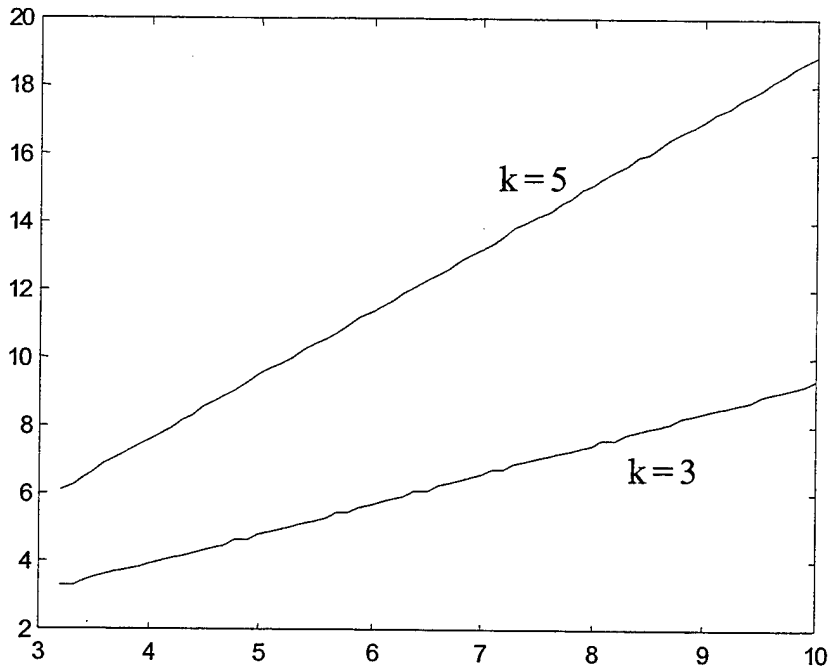


Figure 7. $\dot{\phi}_3/\omega_R$ and $\dot{\phi}_5/\omega_R$ vs. σ for Finned Missile.

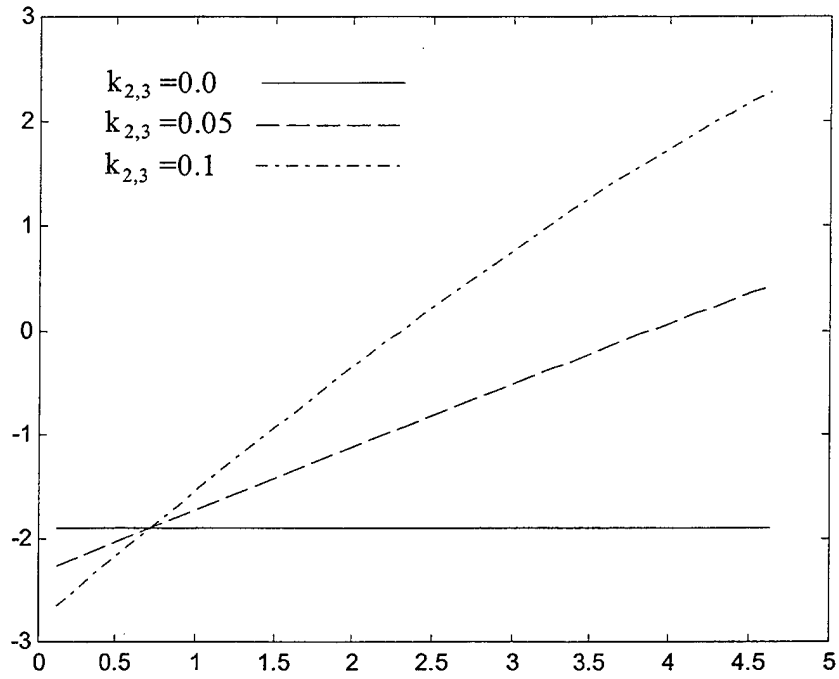


Figure 8. λ_1 vs. p/ω_R for $\sigma = 5$; $k_2 = k_3 = 0, 0.05, \text{ and } 0.10$.

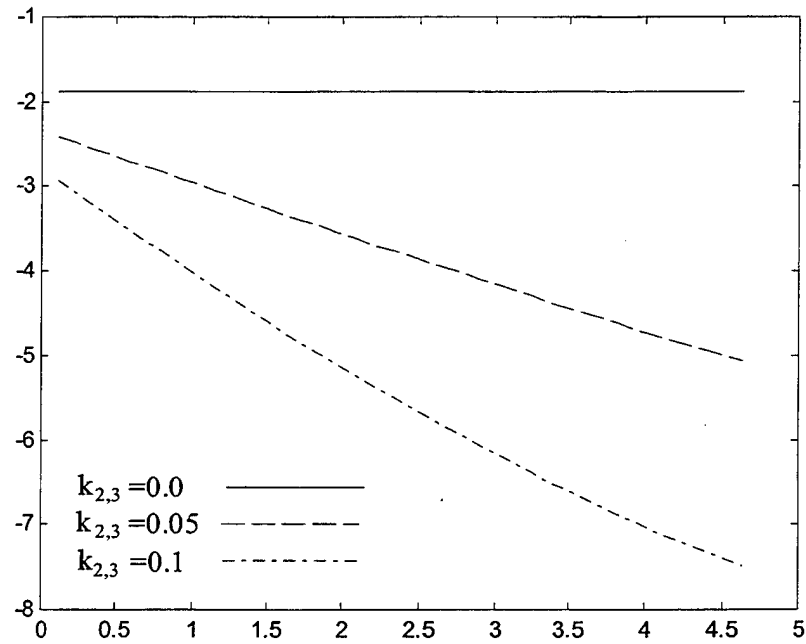


Figure 9. λ_2 vs. p/ω_R for $\sigma = 5$; $k_2 = k_3 = 0, 0.05, \text{ and } 0.10$.

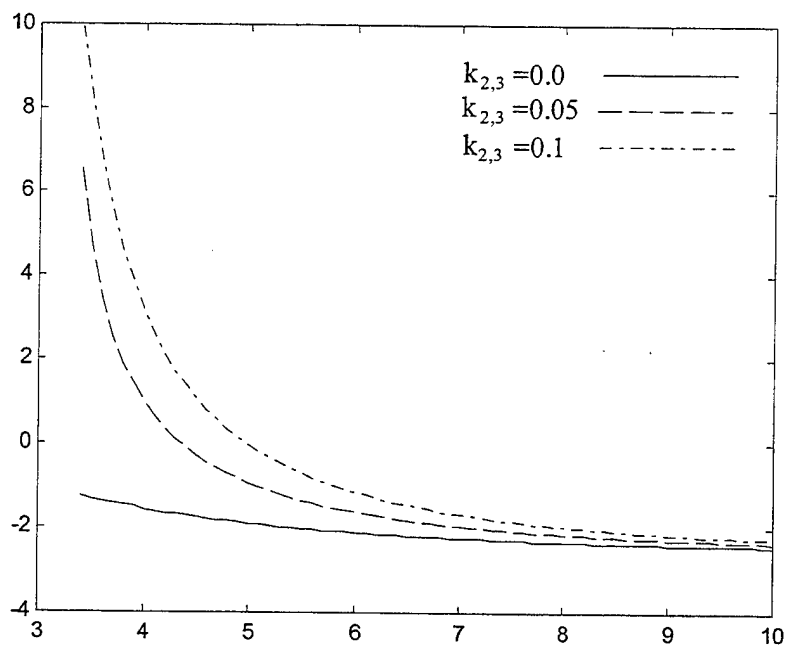


Figure 10. λ_1 vs. σ for $p = 2.3 \omega_R$; $k_2 = k_3 = 0, 0.05$, and 0.10 .

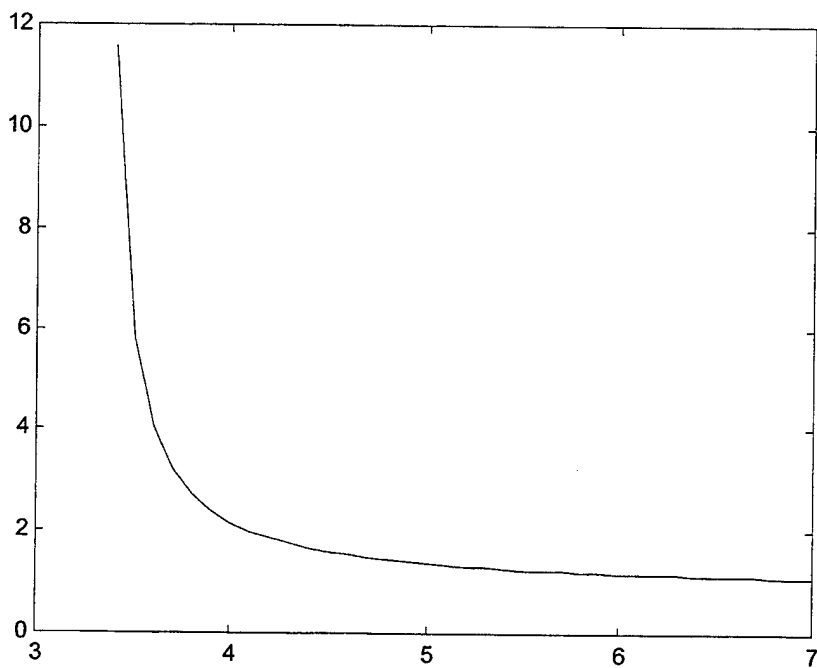


Figure 11. Scaled Zero Spin Trim Angle $|S_{10}|/|S_{10R}|$ vs. σ .

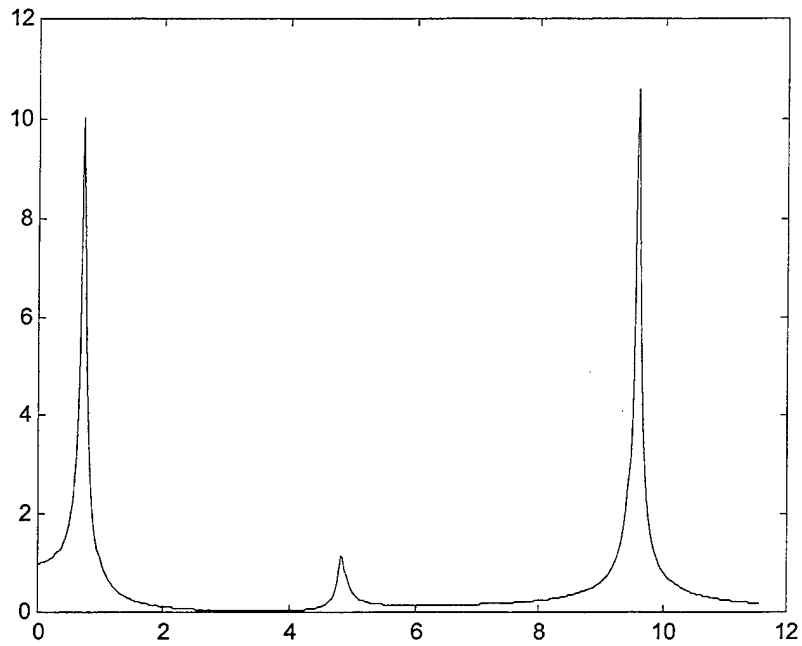


Figure 12(a). $|s_1/s_{10}|$ vs. p/ω_R for $\sigma=5$.

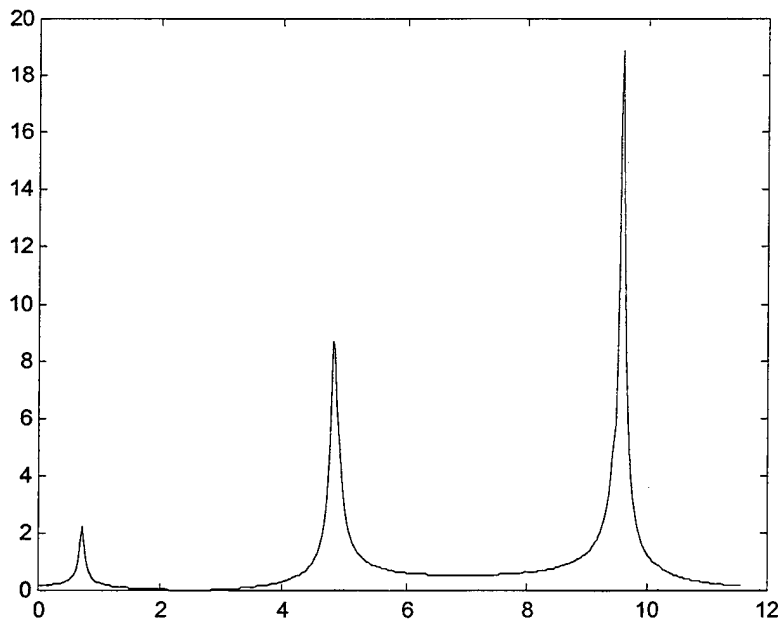


Figure 12(b). $|s_3/s_{10}|$ vs. p/ω_R for $\sigma=5$.

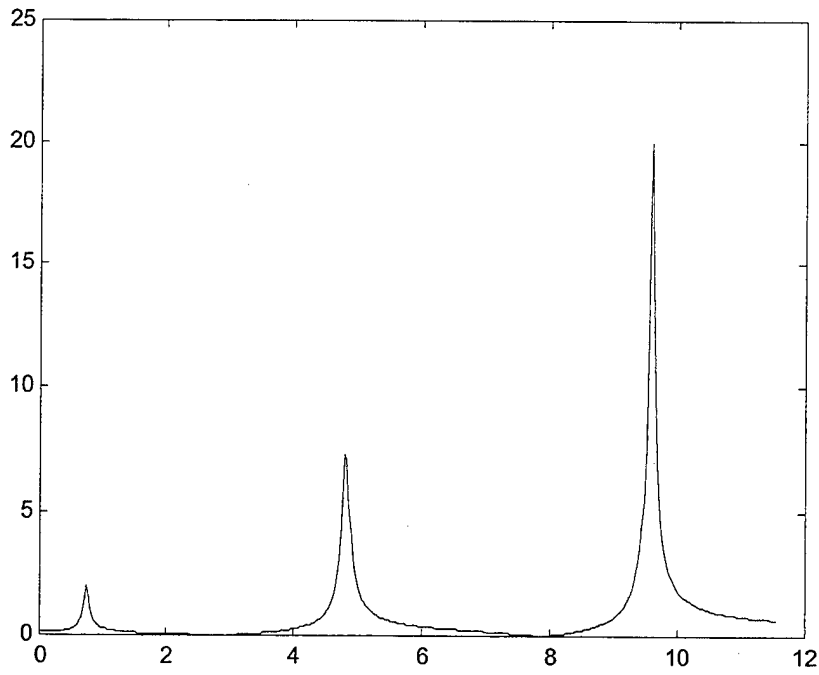


Figure (12)c. $|s_5/s_{10}|$ vs. p/ω_R for $\sigma=5$.

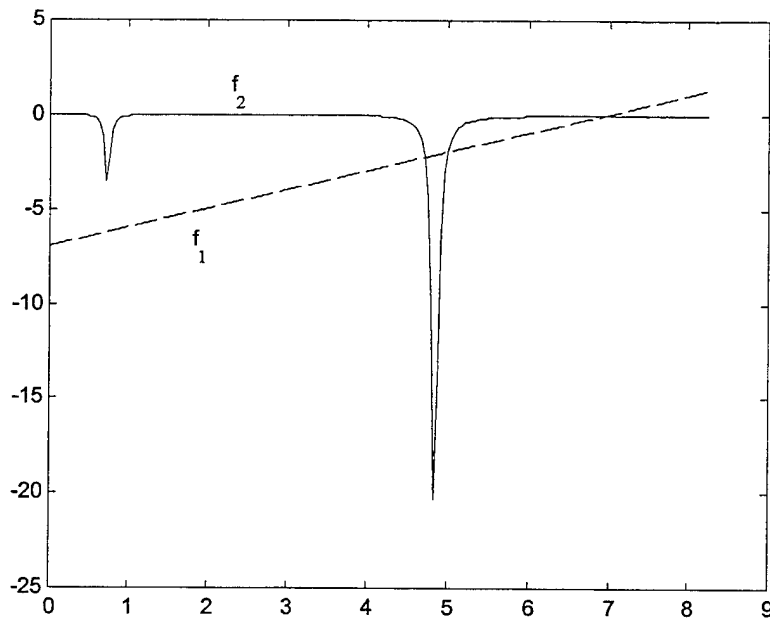


Figure 13. $f_i\omega_R^{-1}$ vs. p/ω_R for Bent Missile With $\sigma=5$; $i=1, 2$.

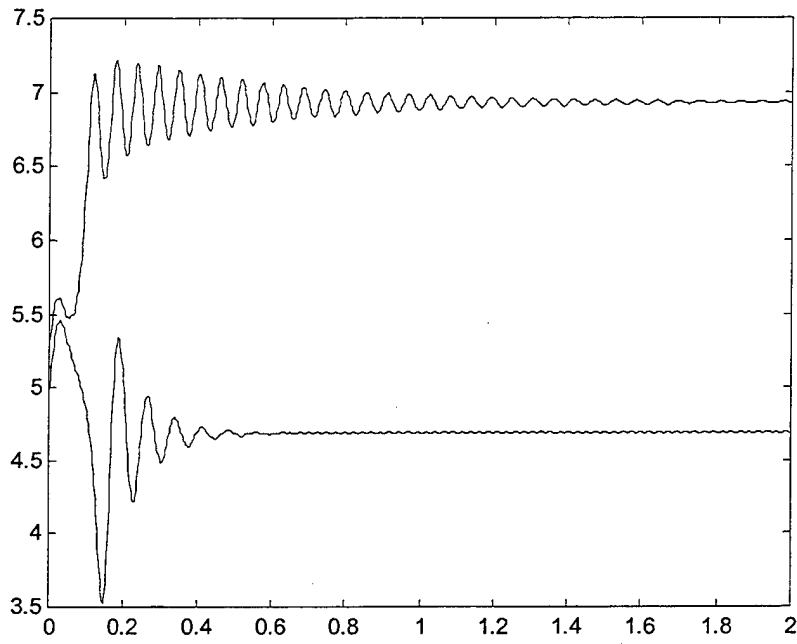


Figure 14. p/ω_R vs. Time for Bent Missile With $\sigma = 5$ ($p_{ss} = 7\omega_R$; $\dot{p}_0 = 4.9\omega_R$; $5.2\omega_R$).

Table 1. Nonerodynamic Matrix Elements

(a) Dynamics Terms	
$R_{11} = I_t$	$R_{41} = -m_3 x_3 d$
$R_{12} = -m_2 (x_2 - x_1) d^2$	$R_{44} = m_3 d$
$R_{13} = -I_{t2}$	$R_{51} = -R_{55} = I_{t3}$
$R_{14} = -m_3 (x_3 - x_1) d^2$	$S_{11}^* = -I_x$
$R_{15} = -I_{t3}$	$S_{13}^* = I_{x2}$
$R_{21} = -m_2 x_2 d$	$S_{15}^* = I_{x3}$
$R_{22} = m_2 d$	$S_{31}^* = -S_{33}^* = -I_{x2}$
$R_{31} = -R_{33} = I_{t2}$	$S_{51}^* = -S_{55}^* = -I_{x3}$
(b) Beam Elastic Terms	
$\hat{T}_{22} = -b_{12} (m_1 + m_2) d / m_1$	$\hat{T}_{42} = -b_{13} m_2 d / m_1$
$\hat{T}_{23} = -b_{22}$	$\hat{T}_{44} = -b_{13} (m_1 + m_3) d / m_1$
$\hat{T}_{24} = -b_{12} m_3 d / m_1$	$\hat{T}_{45} = -b_{23}$
$\hat{T}_{32} = b_{22} (m_1 + m_2) d / m_1$	$\hat{T}_{52} = b_{23} m_2 d / m_1$
$\hat{T}_{33} = b_{32}$	$\hat{T}_{54} = b_{23} (m_1 + m_3) d / m_1$
$\hat{T}_{34} = b_{22} m_3 d / m_1$	$\hat{T}_{55} = b_{33}$
Beam Damping Terms	
$\hat{S}_{22} = -\hat{T}_{22}^* = 2k_2 m_2 \hat{\omega}_2 (m_1 + m_2) d / m_1$	$\hat{S}_{42} = -\hat{T}_{42}^* = 2k_3 m_3 \hat{\omega}_3 m_2 d / m_1$
$\hat{S}_{24} = -\hat{T}_{24}^* = 2k_2 m_2 \hat{\omega}_2 m_3 d / m_1$	$\hat{S}_{44} = -\hat{T}_{44}^* = 2k_3 m_3 \hat{\omega}_3 (m_1 + m_3) d / m_1$

Table 2. Aerodynamic Matrix Elements

\tilde{T}_{nm}	
$\tilde{T}_{11} = -c_3 d$	$\tilde{T}_{23} = -(m - m_2) c_{12} / m$
$\tilde{T}_{12} = -(m_1 c_{D2} - m_2 c_{D1}) d / m_1$	$\tilde{T}_{25} = m_2 c_{13} / m$
$\tilde{T}_{13} = (c_{32} + x_2 c_{12}) d$	$\tilde{T}_{31} = -\tilde{T}_{33} = -c_{32} d$
$\tilde{T}_{14} = -(m_1 c_{D3} - m_3 c_{D1}) d / m_1$	$\tilde{T}_{41} = c_{13} - (m_3 / m) C_{L\alpha}$
$\tilde{T}_{15} = (c_{33} + x_3 c_{13}) d$	$\tilde{T}_{43} = m_3 c_{12} / m$
$\tilde{T}_{21} = c_{12} - (m_2 / m) C_{L\alpha}$	$\tilde{T}_{45} = -(m - m_3) c_{13} / m$
	$\tilde{T}_{51} = -\tilde{T}_{55} = -c_{33} d$
\tilde{S}_{nm}	
$\tilde{S}_{11} = -(c_4 - g_t C_{L\alpha}) d$	$\tilde{S}_{33} = (c_{42} - g_{12} c_{12}) d$
$\tilde{S}_{12} = -(c_{32} + x_2 c_{12}) d$	$\tilde{S}_{35} = -g_{12} c_{13} d$
$\tilde{S}_{13} = (c_{42} + x_2 c_{22} - g_t c_{12}) d$	$\tilde{S}_{41} = (c_{23} - x_3 c_{13} - m_3 x_3 C_{L\alpha} / m)$
$\tilde{S}_{14} = -(c_{33} + x_3 c_{13}) d$	$\tilde{S}_{42} = -m_3 c_{12} / m$
$\tilde{S}_{15} = (c_{43} + x_3 c_{23} - g_t c_{13}) d$	$\tilde{S}_{43} = m_3 x_3 c_{12} / m$
$\tilde{S}_{21} = (c_{22} - x_2 c_{12} - m_2 x_2 C_{L\alpha} / m)$	$\tilde{S}_{44} = (m - m_3) c_{13} / m$
$\tilde{S}_{22} = (m - m_2) c_{12} / m$	$\tilde{S}_{45} = (m_3 x_3 / m) c_{13} - c_{23}$
$\tilde{S}_{23} = (m_2 x_2 / m) c_{12} - c_{22}$	$\tilde{S}_{51} = -(c_{43} - x_3 c_{33} - g_{13} C_{L\alpha}) d$
$\tilde{S}_{24} = -m_2 c_{13} / m$	$\tilde{S}_{53} = -g_{13} c_{12} d$
$\tilde{S}_{25} = m_2 x_2 c_{13} / m$	$\tilde{S}_{54} = -c_{33} d$
$\tilde{S}_{32} = -c_{32} d$	$\tilde{S}_{55} = (c_{43} - g_{13} c_{13}) d$

Table 2. Aerodynamic Matrix Elements (continued)

\tilde{S}_{nm}	
where $g_i = I_i/md^2$; $g_{i2} = I_{i2}/md^2$; and $g_{i3} = I_{i3}/md^2$.	
\tilde{T}_{nm}^*	
$\tilde{T}_{11}^* = -(g_x C_{L\alpha} + c_3^*)d$	$\tilde{T}_{35}^* = g_{x2} c_{13} d$
$\tilde{T}_{13}^* = (g_x c_{12} + c_{32}^* + x_2 c_{12}^*)d$	$\tilde{T}_{51}^* = -(g_{x3} C_{L\alpha} - c_{33}^*)d$
$\tilde{T}_{15}^* = (g_x c_{13} + c_{33}^* + x_3 c_{13}^*)d$	$\tilde{T}_{53}^* = g_{x3} c_{12} d$
$\tilde{T}_{31}^* = -(g_{x2} C_{L\alpha} - c_{32}^*)d$	$\tilde{T}_{55}^* = (g_{x3} c_{13} - c_{33}^*)d$
$\tilde{T}_{33}^* = (g_{x2} c_{12} - c_{32}^*)d$	
where $g_x = I_x/md^2$; $g_{x2} = I_{x2}/md^2$; and $g_{x3} = I_{x3}/md^2$.	

Table 3. Flare-Stabilized Rod Parameters

$m = 2.40$ slug	$a = b = 1.875$ ft
$m_2 = m_3 = 0.60$ slug	$\rho = 0.002$ slug/ft ²
$I_x = 0.0132$ slug-ft ²	$V = 18,000$ ft/s
$I_{x2} = I_{x3} = 0.0033$ slug-ft ²	$c_1 = c_{13} = 2$
$I_t = 5.00$ slug-ft ²	$c_3 = -5$
$I_{t2} = I_{t3} = 0.0781$ slug-ft ²	$c_{33} = -0.32$
$L = 5$ ft	all other c 's are zero
$x_2 = -x_3 = 2.34$ cal	$I_1 = 1.176 \times 10^6$ lb/ft
$(EI)_2 = (EI)_3$	$I_4 = 2.550 \times 10^6$ lb-ft
$d = 0.80$ ft	$I_6 = 4.609 \times 10^6$ lb/ft
$d_{rod} = 0.20$ ft	$M_1 = 18.36$ slug
$I_1 = g_1 d^{-1} \int_{-l/2}^{l/2} \frac{dC_{N\alpha}}{dx} \Psi_1 dx$	$I_6 = g_1 d^{-1} \int_{-l/2}^{l/2} \frac{dC_{N\alpha}}{dx} \Psi_1' \Psi_1 dx$
$I_4 = g_1 d \int_{-l/2}^{l/2} x \frac{dC_{N\alpha}}{dx} \Psi_1' dx$	$M_1 = (m/L) \int_{-l/2}^{l/2} (\Psi_1)^2 dx$

Table 4. Finned Missile Parameters

$m = 3.50$ slug	$c_{D3} = 0.18$
$m_2 = m_3 = 0.875$ slug	$c_1 = 9.4$
$I_x = 0.054$ slug - ft ²	$c_3 = -34.4$
$I_{x2} = I_{x3} = 0.0135$ slug-ft ²	$c_4 = -750$
$I_t = 14.20$ slug-ft ²	$c_{12} = 2.3$
$I_{t2} = I_{t3} = 0.22$ slug-ft ²	$c_{13} = 7.1$
$x_2 = -x_3 = 7.5$ cal	$c_{22} = 19$
$(EI)_2 = (EI)_3$	$c_{23} = 27$
$d = 0.35$ ft	$c_{32} = 5.4$
$a = b = 2.63$ ft	$c_{33} = -3.6$
$\rho = 0.002$ slug/ft ³	$c_{42} = -30$
$V = 6,000$ ft /s	$c_{43} = -10$
$C_D = 0.40$	$c_{43} = -10$
$c_{D2} = 0.15$	all other c_j are zero

Table 5. Bent Missile Terms

(a) Values of $t_{nD}, t_{nD}^*, t_{nA}, t_{nA}^*$	
$t_{1D} = R_{12}E_{2B} + R_{13}\Gamma_{2B} + R_{14}E_{3B} + R_{15}\Gamma_{3B}$	$t_{1D}^* = S_{13}^*\Gamma_{2B} + S_{15}^*\Gamma_{3B}$
$t_{2D} = R_{22}E_{2B}$	$t_{2D}^* = 0$
$t_{3D} = R_{33}\Gamma_{2B}$	$t_{3D}^* = S_{33}^*\Gamma_{2B}$
$t_{4D} = R_{44}E_{3B}$	$t_{4D}^* = 0$
$t_{5D} = R_{55}\Gamma_{3B}$	$t_{5D}^* = S_{55}^*\Gamma_{3B}$
$t_{1A} = -\tilde{T}_{12}E_{2B} - \tilde{T}_{13}\Gamma_{2B} - \tilde{T}_{14}E_{3B} - \tilde{T}_{15}\Gamma_{3B}$ $- [c_{33}\Gamma_{3M} + x_3c_{13}\Gamma_{3F}]d$	$t_{1A}^* = -\tilde{S}_{12}E_{2B} - (\tilde{S}_{13} + \tilde{T}_{13}^*)\Gamma_{2B} - \tilde{S}_{14}E_{3B}$ $- (\tilde{S}_{15} + \tilde{T}_{15}^*)\Gamma_{3B}$
$t_{2A} = -\tilde{T}_{23}\Gamma_{2B} - \tilde{T}_{25}(\Gamma_{3B} + \Gamma_{3F})$	$t_{2A}^* = -\tilde{S}_{22}E_{2B} - \tilde{S}_{23}\Gamma_{2B} - \tilde{S}_{24}E_{3B} - \tilde{S}_{25}\Gamma_{3B}$
$t_{3A} = -c_{32}\Gamma_{2B}d$	$t_{3A}^* = -\tilde{S}_{32}E_{2B} - (\tilde{S}_{33} + \tilde{T}_{33}^*)\Gamma_{2B} - \tilde{S}_{34}E_{3B}$ $- (\tilde{S}_{35} + \tilde{T}_{35}^*)\Gamma_{3B}$
$t_{4A} = -\tilde{T}_{43}\Gamma_{2B} - \tilde{T}_{45}(\Gamma_{3B} + \Gamma_{3F})$	$t_{4A}^* = -\tilde{S}_{42}E_{2B} - \tilde{S}_{43}\Gamma_{2B} - \tilde{S}_{44}E_{3B} - \tilde{S}_{45}\Gamma_{3B}$
$t_{5A} = -c_{33}(\Gamma_{3B} + \Gamma_{3M})d$	$t_{5A}^* = -\tilde{S}_{52}E_{2B} - (\tilde{S}_{53} + \tilde{T}_{53}^*)\Gamma_{2B} - \tilde{S}_{54}E_{3B}$ $- (\tilde{S}_{55} + \tilde{T}_{55}^*)\Gamma_{3B}$
(b) Trim values of E_j, Γ_j	
$E_{2T} = s_2 + E_{2B}$	$\Gamma_{2T} = s_3 + \Gamma_{2B}$
$E_{3T} = s_4 + E_{3B}$	$\Gamma_{3T} = s_5 + \Gamma_{3B}$

Table 6. s_j/s_{10} for Resonant Spins, $\sigma = 5$

p	$0.74\omega_R$	$4.87\omega_R$	$9.72\omega_R$
mag (s_1/s_{10})	10.0	1.2	10.9
mag (s_2/s_{10})	4.9	22.1	90.1
mag (s_3/s_{10})	2.2	8.8	19.5
mag (s_4/s_{10})	4.7	16.2	93.3
mag (s_5/s_{10})	2.0	7.3	20.6
arg (s_1/s_{10})	-87.3°	106.0°	-104.0°
arg (s_2/s_{10})	93.3°	102.6°	-103.8°
arg (s_3/s_{10})	92.7°	102.4°	-103.6°
arg (s_4/s_{10})	91.8°	102.4°	75.6°
arg (s_5/s_{10})	-87.8°	-77.5°	-104.6°

INTENTIONALLY LEFT BLANK.

11. References

1. Fowler, R. H., J. L. Gallop, C. N. H. Lock, and H. W. Richmond. "Aerodynamics of a Spinning Shell." *Philosophical Transactions of Royal Society of London (A)*, vol. 221, pp. 295-387, 1920.
2. McShane, E. J., J. L. Kelley, and F. Reno. *Exterior Ballistics*. Denver, CO: University of Denver Press, 1953.
3. Nicolaides, J. D. "On the Free Flight Motion of Missiles Having Slight Configurational Asymmetries." U.S. Army Ballistic Research Laboratories Report 858, U.S. Army Ballistic Research Laboratories, Aberdeen Proving Ground, MD, June 1953; see also Institute of Aeronautical Sciences Preprint 395, January 1953.
4. Murphy, C. H. "Free Flight Motion of Symmetric Missiles." BRL-TR-1216, U.S. Army Ballistic Research Laboratories, Aberdeen Proving Ground, MD, July 1963.
5. Platus, D. H. "Ballistic Re-entry Vehicle Flight Dynamics." *Journal of Guidance and Control*, vol. 5, pp. 4-16, January-February 1982.
6. Murphy, C. H. "Symmetric Missile Dynamic Instabilities." *Journal of Guidance and Control*, vol. 4, no. 1, pp. 464-471, September-October 1981.
7. Murphy, C. H., J. W. Bradley, and W. H. Mermagen. "Side Moment Exerted by a Spinning, Coning, Highly Viscous Liquid Payload." BRL-TR-3074, U.S. Army Ballistic Research Laboratory, Aberdeen Proving Ground, MD, December 1989.
8. Platus, D. H. "Aeroelastic Stability of Slender, Spinning Missiles." *Journal of Guidance, Control, and Dynamics*, vol. 15, pp. 144-151, January-February 1992.
9. Chadwick, W. R. "Stability of Spinning Shell." Unpublished NSWC report, Naval Surface Weapons Center, Dahlgren, VA, September 1975.
10. Murphy, C. H. "Spinning Projectile Instability Induced by an Internal Mass Mounted on an Elastic Beam." ARL-MR-270, U.S. Army Research Laboratory, Aberdeen Proving Ground, MD, November 1995; see also *AIAA* paper 92-4493CP, August 1992.
11. Murphy, C. H. "Some Special Cases of Spin-Yaw Lock-In." *Journal of Guidance, Control, and Dynamics*, vol. 12, pp. 771-776, November-December 1989; see also BRL-MR-3609, U.S. Army Ballistic Research Laboratory, Aberdeen Proving Ground, MD, August 1987.
12. Geradin, M., and D. Rixen. *Mechanical Vibrations*. New York: John Wiley, 1997.

INTENTIONALLY LEFT BLANK.

Appendix A:
Aerodynamic Properties of
Finned Missile

INTENTIONALLY LEFT BLANK.

Our finned missile is assumed to have uniform mass distribution over a 20-cal.-long cylinder with the density of aluminum. The external configuration has a fineness ratio of 22 due a very light conical windshield of 1 cal. and a 1-cal. extension of the four fins past the cylinder base (Figure A-1). The centers of mass of the three components are located at x_j , and these locations can be computed in terms of the lengths of the cylindrical segments.

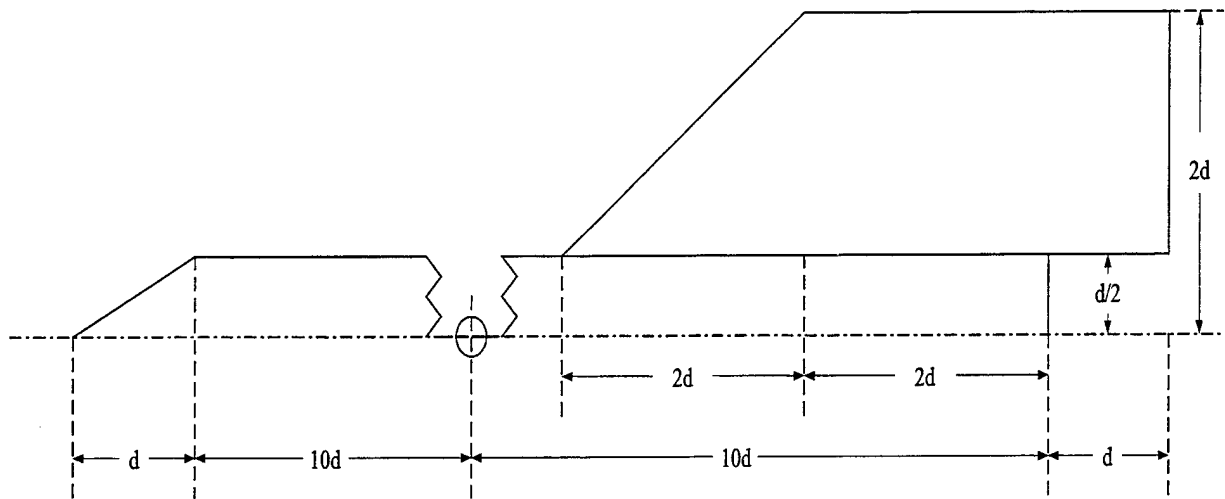


Figure A-1. Sketch of a Hypersonic Missile.

$$x_1 = (L_3 - L_2)/2 \quad ; x_2 = (L - L_2)/2 \quad ; x_3 = -(L - L_3)/2. \quad (\text{A-1})$$

In Wood and Murphy,¹ the slender distribution of normal force coefficient is shown to be:

$$\left[\frac{dC_N}{dx} \right] = -\frac{2}{S} \left[\alpha_j \frac{dA}{dx} - \frac{\dot{\alpha}_j A d}{V} - \frac{\dot{\theta} d}{V} \left(A + (x - x_j) \frac{dA}{dx} \right) + \frac{\ddot{\theta} d^2}{V^2} x A \right]; \quad -10 \leq x \leq 11, \quad (\text{A-2})$$

where A is the body crosssectional area and α_j is angle of attack at x_j .

¹ Wood, R. M., and C. H. Murphy. "Aerodynamic Derivatives of Both Steady and Nonsteady Motion of Slender Bodies." *Journal of the Aeronautical Sciences*, vol. 22, pp. 870-871, December 1955; see also BRL-MR-880, U.S. Army Ballistic Research Laboratories, Aberdeen Proving Ground, MD, April 1955.

For the flight dynamics of this report, $\dot{\alpha} = \dot{\theta}$ and the $\ddot{\theta}$ term have no effect.

$$\left[\frac{dC_N}{dx} \right]_{body} = -\frac{2}{S} \left[\alpha_j \frac{dA}{dx} - \frac{\dot{\alpha}_j d}{V} \left(2A + (x - x_j) \frac{dA}{dx} \right) \right] ; -10 \leq x \leq 11. \quad (A-3)$$

This expression usually underestimates $C_{N\alpha}$ by 30% due to its prediction of no normal force acting on the constant area cylinder. Therefore, we add a cylinder normal force term.

$$\left[\frac{dC_N}{dx} \right]_{cylinder} = 0.6 \left[\alpha_j - (x - x_j) (\dot{\alpha} d / V) \right] e^{x-10} ; x \leq 10. \quad (A-4)$$

The contribution of the fins can be estimated by the "strip" theory of Boltz and Nicolaidis,² which is based on the two-dimensional linear supersonic theory for the two fins in the x-z plane.

$$\left[\frac{dC_N}{dx} \right]_{fins} = 2(a_L d^2 / S)(y_f - 0.5) \left[\alpha_j - (x - x_j) (\dot{\alpha} d / V) \right], \quad (A-5)$$

where

$$y_f = -\frac{(13 + 3x)}{4} \quad -7 \leq x \leq -5,$$

$$= 2 \quad -11 \leq x \leq -7$$

$$a_L = 2 \left[\sqrt{M^2 - 1} \right]^{-1} ; M = \text{Mach number.}$$

$(dC_{N\alpha}/dx)$ is the sum of three coefficients of α_j in equations A-3 through A-5. $(C_N)_j$ can be obtained by integrating the sum of equations A-4 through A-6 over the i-th component.

$$(C_N)_1 = \int_{-5}^5 \left[\frac{dC_N}{dx} \right] dx = c_{11} \xi_1 + c_{21} \left(\dot{\xi}_1 d / V \right). \quad (A-6)$$

² Boltz, R. E., and J. D. Nicolaidis. "A Method of Determining Some Aerodynamic Coefficients From Supersonic Free Flight Tests of a Rolling Missile." *Journal of the Aeronautical Sciences*, vol. 17, pp. 609-629, October 1950.

$$(C_N)_2 = \int_5^{11} \left[\frac{dC_N}{dx} \right] dx = c_{12} \xi_2 + c_{22} (\dot{\xi}_2 d/V). \quad (\text{A-7})$$

$$(C_N)_3 = \int_{-11}^{-5} \left[\frac{dC_N}{dx} \right] dx = c_{13} \xi_3 + c_{23} (\dot{\xi}_3 d/V). \quad (\text{A-8})$$

$(C_M)_j$ can now be obtained by multiplying the sum of equations A-3 through A-5 by $(x - x_j)$ and integrating the result over the j-th component. In Table 4, these relations were used to compute c_{ij} for $L_2 = L_3 = L/2$.

Finally, the roll damping moment, $C_{\ell p}$, was computed from $(dC_N/dx)_{fns}$ using the local angle of attack due to spin.

$$C_{\ell p}(pd/V) = -4(\alpha_L d^3/S) \int_{-11}^{-5} (y_f - 0.5) [p(y_f + 0.5)/2V] dx. \quad (\text{A-9})$$

INTENTIONALLY LEFT BLANK.

Appendix B:
Internal Beam-Supported Mass

INTENTIONALLY LEFT BLANK.

Chadwick¹ and Murphy² studied the effect of beam damping on the dynamic stability of a spinning projectile with a beam-mounted symmetric mass and aerodynamic damping. These references showed that beam damping could cause dynamic instability when the beam's elastic frequency is near the projectile's fast pitch frequency. The effect of an internal cantilever beam-supported asymmetric mass on the motion of a spinning projectile, however, was first studied by Reed³ for no aerodynamic or elastic damping. He showed that dynamic instability would occur when the elastic frequency was near the projectile's slow pitch frequency and that large resonant motion would occur for spins near the cantilever beam elastic frequency.

The equations of this report can be used to study the complete problem for both symmetric and asymmetric masses. Table B-1 gives the necessary parameters for the projectile studied by Murphy.⁴ In Figure B-1, we plot λ_1 vs. $\hat{\omega}_3/\dot{\phi}_{1R}$ for different beam damping, $k_3 = 0, 0.1, 0.2$. We see that dynamic instability does occur near $\hat{\omega}_3 = \dot{\phi}_{1R}$ when k_3 is 0.2. Figure B-2 shows the damping of the slow frequency, λ_2 , as a function of $\hat{\omega}_3/\dot{\phi}_{2R}$. We see that this mode is unstable near $\hat{\omega}_3 = \dot{\phi}_{2R}$ as was predicted by Reed. In Figure B-3, we plot ξ_T and E_{3T} vs. $p/\hat{\omega}_3$. Resonance occurs for $p = 1.07\hat{\omega}_3$, and this large beam deflection was predicted by Reed. This analysis can be extended to other beam types, pinned, fixed-fixed, etc., by using the beam influence coefficients given by Chadwick and Murphy.

¹ Chadwick, W. R. "Stability of Spinning Shell." Unpublished NSWC Report, Naval Surface Weapons Center, Dahlgren, VA, September 1975.

² Murphy, C. H. "Spinning Projectile Instability Induced by an Internal Mass Mounted on an Elastic Beam." ARL-MR-270, U.S. Army Research Laboratory, Aberdeen Proving Ground, MD, November 1995; see also *AIAA* paper 92-4493CP, August 1992.

³ Reed, H. L. "On the Motion of a Shell With an Internally Mounted Cantilever Beam." BRL-TR-1039, U.S. Army Ballistic Research Laboratories, Aberdeen Proving Ground, MD, November 1957.

⁴ Murphy, C. H. "Influence of Moving Interior Parts on the Angular Motion of Spinning Projectiles." *Journal of Guidance and Control*, vol. 1, no. 2, pp. 117-122, March-April 1978; see also BRL-MR-2731, U.S. Army Ballistic Research Laboratories, Aberdeen Proving Ground, MD, February 1977.

Table B-1. Parameters for Spinning Projectile With Interior Beam-Mounted Mass

$m_2 = I_{x2} = I_{t2} = 0$	$d = 0.6667$ ft
$x_2 = k_2 = c_{ij} = 0$	$a = 0.50$ ft
$p = 637$ rad/s	$b = 1.16$ ft
$m = 22.6$ slug	$\rho = 0.0020$ slug/ft ³
$m_3 = 2.6$ slug	$V = 1,200$ ft/s
$I_x = 0.370$ slug-ft ²	$c_1 = 2.5$
$I_{x3} = 0.130$ slug-ft ²	$C_D = 0.5$
$I_t = 2.610$ slug-ft ²	$c_3 = 5.0$
$I_{t3} = 0.070$ slug-ft ²	$c_4 = -5.0$
$x_3 = -0.45$ cal.	$c_1^* = c_2^* = c_4^* = 0$
$E_{3B} = 0.002$	$c_3^* = 0.10$
$\Gamma_{3B} = 0$	—

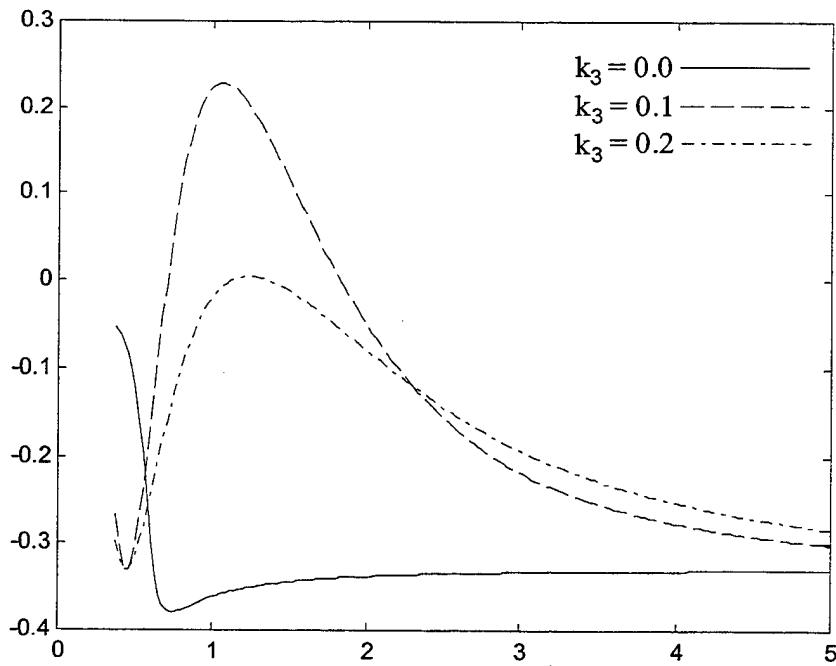


Figure B-1. λ_1 vs. $\hat{\omega}_3 / \dot{\phi}_{1R}$.

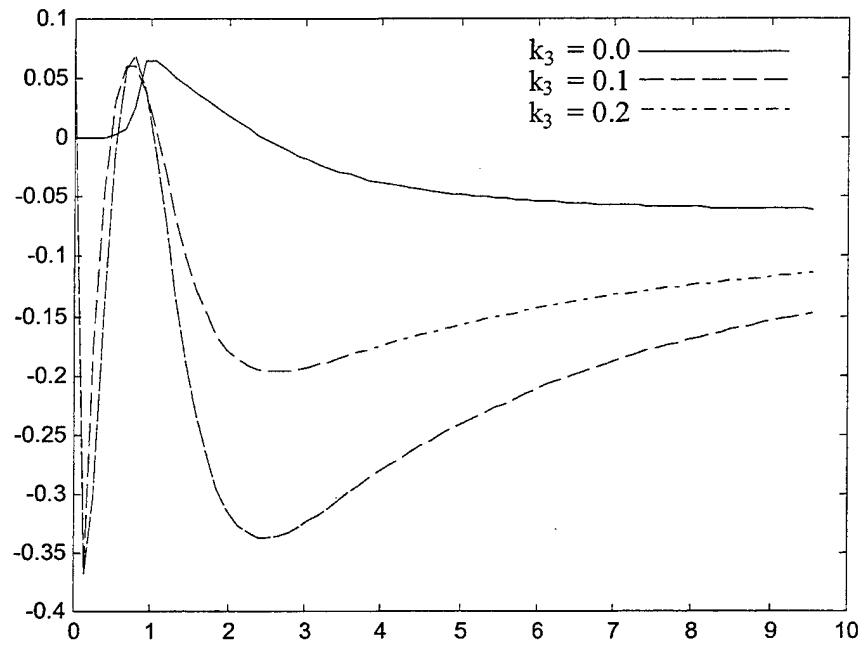


Figure B-2. λ_2 vs. $\hat{\omega}_3 / \dot{\phi}_{2R}$.

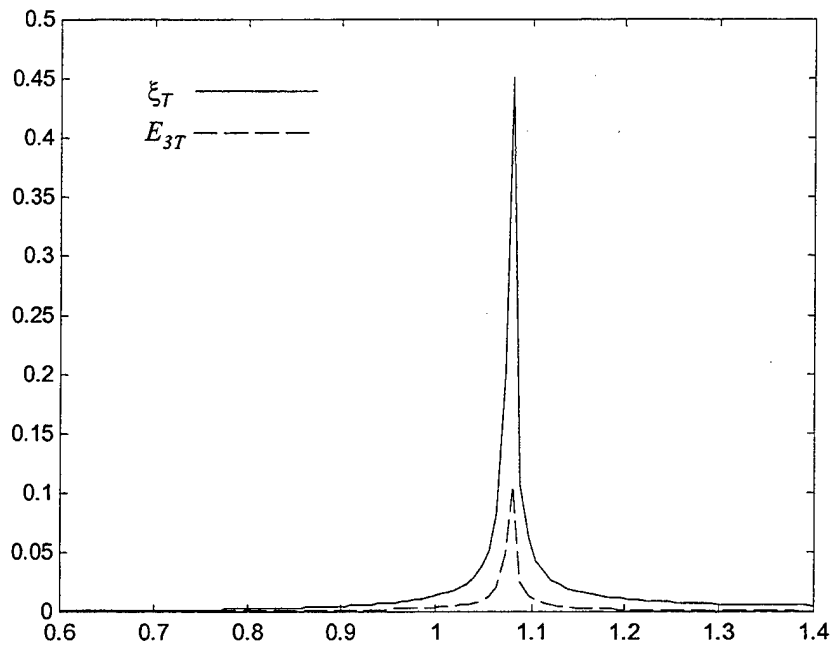


Figure B-3. $|\xi_T|$ and $|E_{3T}|$ vs. $p / \hat{\omega}_3$.

INTENTIONALLY LEFT BLANK.

List of Symbols

d	projectile diameter
E_j	dimensionless complex lateral location of cm of body j with respect to projectile cm
$(EI)_j$	stiffness of beam attached to body j
g_1	$\rho V^2 S/2$
\vec{H}_j	angular momentum vector of body j
I_x	axial moment of inertia of projectile
I_{xj}	axial moment of inertia of body j
I_t	transverse moment of inertia of projectile
I_{tj}	transverse moment of inertia of body j
L_j	dimensionless length of body j , i.e., fineness ratio
m	projectile mass
m_j	mass of body j
p	p_1 , projectile spin
p_j	axial component of angular velocity of body j
Q	$\dot{\theta} + i\dot{\psi}$, complex angular velocity of body 1
r_m	m_2/m , mass ratio
S	$\pi d^2/4$
V	magnitude of projectile velocity
x_j	dimensionless axial location of cm of body j with respect to the cm of the projectile

α	angle of attack at the projectile cm
β	angle of sideslip at the projectile cm
ϕ	roll angle of body 1
$\dot{\phi}_k$	frequency of k-th mode
λ_k	damping of k-th mode
θ	pitch angle of body 1
ρ	air density
σ	$\omega/\dot{\phi}_{1R}$
$\hat{\omega}$	common value of beam frequency when $\hat{\omega}_2 = \hat{\omega}_3$
$\hat{\omega}_2$	$\sqrt{3(EI)_2/(m_1 m_2 a^3)}$
$\hat{\omega}_3$	$\sqrt{3(EI)_3/(m_1 m_2 b^3)}$
ω_K	K-th frequency for free-free uniform elastic beam
ω_R	$\sqrt{T_{11}/I_t}$, rigid projectile zero-spin frequency
ξ	$\beta + i\alpha$, complex angle of attack of projectile
$\Psi_K(x)$	K-th eigenfunction for free-free uniform elastic beam
ψ	yaw angle of body 1
(F_{xj}, F_{yj}, F_{zj})	aerodynamic force exerted on body j
$(\hat{F}_{xj}, \hat{F}_{yj}, \hat{F}_{zj})$	elastic beam force exerted on body j
(M_{xj}, M_{yj}, M_{zj})	aerodynamic moment exerted on body j
$(\hat{M}_{xj}, \hat{M}_{yj}, \hat{M}_{zj})$	elastic beam moment exerted on body j

- (v_{xj}, v_{yj}, v_{zj}) velocity of body j
- (X_j, Y_j, Z_j) location of cm of body j with respect to the cm of body 1
- $(\Gamma_{yj}, \Gamma_{zj})$ pitch and yaw angles of body j with respect to body 1
- $R\{z\}$ real part of z
- $I\{z\}$ imaginary part of z

NOTES:

- Tilde superscript denotes quantity related to elastic beam.
- Circumflex superscript denotes aerodynamic quantity.
- e subscript denotes earth-fixed axes.
- B subscript denotes parameter for bent projectile.
- R subscript denotes parameter for rigid symmetric projectile.

INTENTIONALLY LEFT BLANK.

<u>NO. OF COPIES</u>	<u>ORGANIZATION</u>
2	DEFENSE TECHNICAL INFORMATION CENTER DTIC OCA 8725 JOHN J KINGMAN RD STE 0944 FT BELVOIR VA 22060-6218
1	HQDA DAMO FDT 400 ARMY PENTAGON WASHINGTON DC 20310-0460
1	OSD OUSD(A&T)/ODDR&E(R) DR R J TREW 3800 DEFENSE PENTAGON WASHINGTON DC 20301-3800
1	COMMANDING GENERAL US ARMY MATERIEL CMD AMCRDA TF 5001 EISENHOWER AVE ALEXANDRIA VA 22333-0001
1	INST FOR ADVNCD TCHNLGY THE UNIV OF TEXAS AT AUSTIN 3925 W BRAKER LN STE 400 AUSTIN TX 78759-5316
1	DARPA SPECIAL PROJECTS OFFICE J CARLINI 3701 N FAIRFAX DR ARLINGTON VA 22203-1714
1	US MILITARY ACADEMY MATH SCI CTR EXCELLENCE MADN MATH MAJ HUBER THAYER HALL WEST POINT NY 10996-1786
1	DIRECTOR US ARMY RESEARCH LAB AMSRL D DR D SMITH 2800 POWDER MILL RD ADELPHI MD 20783-1197

<u>NO. OF COPIES</u>	<u>ORGANIZATION</u>
1	DIRECTOR US ARMY RESEARCH LAB AMSRL CI AI R 2800 POWDER MILL RD ADELPHI MD 20783-1197
3	DIRECTOR US ARMY RESEARCH LAB AMSRL CI LL 2800 POWDER MILL RD ADELPHI MD 20783-1197
3	DIRECTOR US ARMY RESEARCH LAB AMSRL CI AP 2800 POWDER MILL RD ADELPHI MD 20783-1197
	<u>ABERDEEN PROVING GROUND</u>
2	DIR USARL AMSRL CI LP (BLDG 305)

<u>NO. OF COPIES</u>	<u>ORGANIZATION</u>	<u>NO. OF COPIES</u>	<u>ORGANIZATION</u>
1	COMMANDER US ARMY ARDEC TECHNICAL LIBRARY PICATINNY ARSENAL NJ 07806-5000	3	COMMANDER US ARMY ARDEC SMCAR CCH V B KONRAD E FENNELL T LOUZERIO PICATINNY ARSENAL NJ 07806-5000
1	COMMANDER US NAVAL SURFACE WEAPONS WARFARE CENTER T PEPITONE MS MC K21 DAHLGREN VA 22448	4	COMMANDER US ARMY ARDEC SMCAR FSE A GRAF D LADD E ANDRICOPOULIS K CHEUNG PICATINNY ARSENAL NJ 07806-5000
1	TECHNICAL DIRECTOR US ARMY ARDEC AMSTA AR TD M FISSETTE PICATINNY ARSENAL NJ 07806-5000	6	COMMANDER US ARMY ARDEC SMCAR CCL D F PUZYCKI D CONWAY D DAVIS K HAYES M PINCAY W SCHUFF PICATINNY ARSENAL NJ 07806-5000
1	PRINCIPAL DPTY FOR TECHNOLOGY HEADQUARTERS US ARMY MATERIEL COMMAND C W KITCHENS ALEXANDRIA VA 22333-0001	2	COMMANDER US ARMY ARDEC SMCAR DSD T R LIESKE F MIRABELLE ABERDEEN PROVING GROUND MD 21005
12	COMMANDER US ARMY ARDEC AET A C NG J GRAU S KAHN H HUDGINS M AMORUSO E BROWN B WONG W TOLEDO S CHUNG C LIVECCHIA G MALEJKO J WHYTE PICATINNY ARSENAL NJ 07806-5000	3	DIRECTOR US ARMY RESEARCH OFFICE G ANDERSON K CLARK T DOLIGOWSKI PO BOX 12211 RESEARCH TRIANGLE PARK NC 27709-2211

<u>NO. OF COPIES</u>	<u>ORGANIZATION</u>
1	COMMANDER CODE DK20 MOORE CODE DK20 DEVAN US NAVAL SURFACE WEAPONS CTR DAHLGREN VA 22448-5000
2	COMMANDER CODE R44 F PRIOLO CODE R44 A WARDLAW US NSWC APPLIED MATH BRANCH WHITE OAK LABORATORY SILVER SPRING MD 20903-5000
1	COMMANDER US ARMY AVIATION AND MISSILE COMMAND AMSAM RD SS AT W WALKER REDSTONE ARSENAL AL 35898-5010
4	COMMANDER US AIR FORCE ARMAMENT LAB AFATL FXA B SIMPSON G ASATE R ABELGREN G WINCHENBACK EGLIN AFB FL 32542-5434
2	DIRECTOR SANDIA NATIONAL LABORATORY W OBERKAMPF W WOLFE DIVISION 5800 ALBUQUERQUE NM 87185
1	DIRECTOR LOS ALAMOS NATIONAL LAB MS G770 W HOGAN LOS ALAMOS NM 87545
1	DIRECTOR NASA AMES RESEARCH CTR MS 258 1 L SCHIFF MOFFETT FIELD CA 94035

<u>NO. OF COPIES</u>	<u>ORGANIZATION</u>
1	DIRECTOR NASA LANGLEY RESEARCH CTR M HEMSCH LANGLEY STATION HAMPTON VA 23665
1	MASSACHUSETTS INST OF TECH DEPT OF AERONAUTICS AND ASTRONAUTICS E COVERT 77 MASSACHUSETTS AVE CAMBRIDGE MA 02139
1	ARROW TECHNOLOGY ASSOCIATES INC R WHYTE PO BOX 4218 BURLINGTON VT 05401-4218
2	C H MURPHY PO BOX 269 UPPER FALLS MD 21156
2	W H MERMAGEN 4149 U WAY HAVRE DE GRACE MD 21078
	<u>ABERDEEN PROVING GROUND</u>
24	DIR USARL AMSRL WM B A HORST AMSRL WM BA W DAMICO T HAWKINS B DAVIS AMSRL WM BC P PLOSTINS V OSKAY J GARNER J SAHU B GUIDOS P WEINACHT G COOPER M BUNDY K SOENCKSEN W DRYSDALE S WILKERSON

NO. OF
COPIES ORGANIZATION

ABERDEEN PROVING GROUND

AMSRL WM BD
T MINOR
AMSRL WM BF
H EDGE
AMSRL HR MB
D SAVICK
AMSRL WM T
B BURNS
AMSRL WM TC
R MUDD
R COATES
W DE ROSSET
AMSRL WM TD
E RAPACKI
AMSRL SL BE
A MIKHAIL

REPORT DOCUMENTATION PAGE			Form Approved OMB No. 0704-0188	
Public reporting burden for this collection of information is estimated to average 1 hour per response, including the time for reviewing instructions, searching existing data sources, gathering and maintaining the data needed, and completing and reviewing the collection of information. Send comments regarding this burden estimate or any other aspect of this collection of information, including suggestions for reducing this burden, to Washington Headquarters Services, Directorate for Information Operations and Reports, 1215 Jefferson Davis Highway, Suite 1204, Arlington, VA 22202-4302, and to the Office of Management and Budget, Paperwork Reduction Project(0704-0188), Washington, DC 20503.				
1. AGENCY USE ONLY (Leave blank)	2. REPORT DATE April 2000	3. REPORT TYPE AND DATES COVERED Final, June 99 - June 00		
4. TITLE AND SUBTITLE Flight Mechanics of an Elastic Symmetric Missile			5. FUNDING NUMBERS 1L162618H80	
6. AUTHOR(S) Charles H. Murphy and William H. Mermagen, Sr.				
7. PERFORMING ORGANIZATION NAME(S) AND ADDRESS(ES) U.S. Army Research Laboratory ATTN: AMSRL-WM-BA Aberdeen Proving Ground, MD 21005-5066			8. PERFORMING ORGANIZATION REPORT NUMBER ARL-TR-2255	
9. SPONSORING/MONITORING AGENCY NAMES(S) AND ADDRESS(ES)			10. SPONSORING/MONITORING AGENCY REPORT NUMBER	
11. SUPPLEMENTARY NOTES				
12a. DISTRIBUTION/AVAILABILITY STATEMENT Approved for public release; distribution is unlimited.			12b. DISTRIBUTION CODE	
13. ABSTRACT (Maximum 200 words) The free-flight motion of an elastic missile is approximated with three bodies connected by two massless elastic cantilever beams. If the mass distribution of the three bodies is 1-2-1, the frequency of the symmetric oscillation of the outer bodies is within 5% of the classical frequency of the oscillation of a free-free beam. A second combined pitching antisymmetric flexing motion can occur with a frequency that is almost twice that of the symmetric flexing motion. As the beam stiffness is reduced, the symmetric flexing motion frequency approaches the rigid body aerodynamic zero-spin frequency, and the flight zero-spin aerodynamic frequency is considerably reduced. Moderate beam damping can cause dynamic instability for spins greater than the zero-spin aerodynamic frequency. Resonance mode amplification can occur when the spin is equal to the zero-spin aerodynamic frequency, but more importantly it can occur when the spin is equal to the two elastic flexing frequencies. Spin-yaw lock-in occurs at the lower elastic frequency.				
14. SUBJECT TERMS flight mechanics, elastic missile, beam damping, spin-yaw lock-in, aeroelastic motion			15. NUMBER OF PAGES 62	
			16. PRICE CODE	
17. SECURITY CLASSIFICATION OF REPORT UNCLASSIFIED	18. SECURITY CLASSIFICATION OF THIS PAGE UNCLASSIFIED	19. SECURITY CLASSIFICATION OF ABSTRACT UNCLASSIFIED	20. LIMITATION OF ABSTRACT UL	

INTENTIONALLY LEFT BLANK.

USER EVALUATION SHEET/CHANGE OF ADDRESS

This Laboratory undertakes a continuing effort to improve the quality of the reports it publishes. Your comments/answers to the items/questions below will aid us in our efforts.

1. ARL Report Number/Author ARL-TR-2255 (POC: Lyon) Date of Report April 2000

2. Date Report Received _____

3. Does this report satisfy a need? (Comment on purpose, related project, or other area of interest for which the report will be used.) _____

4. Specifically, how is the report being used? (Information source, design data, procedure, source of ideas, etc.) _____

5. Has the information in this report led to any quantitative savings as far as man-hours or dollars saved, operating costs avoided, or efficiencies achieved, etc? If so, please elaborate. _____

6. General Comments. What do you think should be changed to improve future reports? (Indicate changes to organization, technical content, format, etc.) _____

CURRENT
ADDRESS

Organization

Name

E-mail Name

Street or P.O. Box No.

City, State, Zip Code

7. If indicating a Change of Address or Address Correction, please provide the Current or Correct address above and the Old or Incorrect address below.

OLD
ADDRESS

Organization

Name

Street or P.O. Box No.

City, State, Zip Code

(Remove this sheet, fold as indicated, tape closed, and mail.)

(DO NOT STAPLE)

DEPARTMENT OF THE ARMY

OFFICIAL BUSINESS

BUSINESS REPLY MAIL

FIRST CLASS PERMIT NO 0001,APG,MD

POSTAGE WILL BE PAID BY ADDRESSEE

DIRECTOR
US ARMY RESEARCH LABORATORY
ATTN AMSRL WM BA
ABERDEEN PROVING GROUND MD 21005-5066



NO POSTAGE
NECESSARY
IF MAILED
IN THE
UNITED STATES

